

# **Vibration Suppression of An Optical Table**

*Tsung-Wun Wang*

*Advisor: Fu-Cheng Wang*

*Department of Mechanical Engineering*

*National Taiwan University*

*Taipei, Taiwan*

June 2022



# Abstract

Vibration control in optical tables is critical for precision applications, necessitating careful design to minimize disturbances. This paper introduces disturbance response decoupling (DRD), focusing on its application to optical table designs, from quarter and half structures to full tables. Our simulations of DRD control strategies demonstrate their effectiveness in decoupling exogenous disturbances and significantly reducing vibrations by implementing suitable stabilizing controllers.

As we extend the optical table design to half and full sizes, we find that the original DRD strategy improves outputs for only one specific disturbance per controller. Therefore, modifications are needed to generalize the relationship between all disturbances and outputs. Consequently, we rename the original DRD architecture as Input DRD (IDRD) and propose two additional strategies: Output DRD (ODRD) and an integrated approach called Input-Output DRD (IODRD). Simulation results indicate substantial decoupling effects and notable vibration reduction. These findings suggest a robust framework for enhancing optical table performance under varied conditions. Future experiments will be designed to validate the ODRD and IODRD strategies.

Keywords: Disturbance Response Decoupling (DRD), Vibration Control, Optical Table, Output DRD (ODRD), Input-Output DRD (IODRD)



# Contents

<b>Abstract</b>	<b>i</b>
<b>List of Figures</b>	<b>vii</b>
<b>List of Tables</b>	<b>xi</b>
<b>Abbreviations and Acronyms</b>	<b>xiii</b>
<b>Notation</b>	<b>xv</b>
<b>1 Related Work</b>	<b>1</b>
1.1 Linear Fractional Transformation . . . . .	1
<b>2 Experimental Setup</b>	<b>3</b>
2.1 Components in An Optical Table . . . . .	3
2.1.1 Vertical Vibration Machine . . . . .	3
2.1.2 Linear Spring . . . . .	3
2.1.3 Piezoelectric Actuator . . . . .	5
2.1.4 Voice Coil Motor . . . . .	7
2.1.5 Accelerometer . . . . .	7
2.1.6 Linear Variable Differential Transformer . . . . .	9
2.1.7 Load Cell . . . . .	11
2.1.8 Multifunction I/O Device . . . . .	13

<b>3</b>	<b>Quarter Table</b>	<b>15</b>
3.1	Dynamics Equations . . . . .	15
3.2	Controller Design . . . . .	17
3.2.1	Design of $\tilde{U}_2$ . . . . .	17
3.2.2	Design of $K_1$ . . . . .	17
3.3	Simulation . . . . .	17
3.3.1	Vibration Reduction . . . . .	20
<b>4</b>	<b>Half Table</b>	<b>23</b>
4.1	Dynamics Equations . . . . .	23
4.2	Controller Design . . . . .	24
4.2.1	Design of $\tilde{U}_2$ . . . . .	24
4.2.2	Design of $K_1$ . . . . .	24
4.3	Simulation - Maximize The Vibration Reduction without Con- strained Stroke of Piezo Actuator . . . . .	26
4.3.1	Vibration Reduction . . . . .	29
4.4	Simulation - Maximize The Vibration Reduction with Limited Stroke of Piezo Actuator . . . . .	29
4.4.1	Vibration Reduction . . . . .	30
<b>5</b>	<b>Full Table</b>	<b>35</b>
5.1	Dynamics Equations . . . . .	35
5.2	Controller Design . . . . .	38
5.2.1	Design of $\tilde{U}_2$ . . . . .	38
5.2.2	Design of $K_1$ . . . . .	38
5.3	Simulation . . . . .	38
5.3.1	Vibration Reduction . . . . .	41
<b>6</b>	<b>Disturbance Response Decoupling</b>	<b>43</b>
6.1	General Control Configuration . . . . .	43
6.2	Review of Controller Parameterization . . . . .	45

6.3	Input Disturbance Response Decoupling (IDRD) . . . . .	46
6.3.1	Q-Parameterization (Youla) . . . . .	46
6.3.2	Decoupling Effect . . . . .	49
6.4	Output Disturbance Response Decoupling (ODRD) . . . . .	52
6.4.1	Q-Parameterization (Youla) . . . . .	52
6.4.2	Decoupling Effect . . . . .	53
<b>7</b>	<b>Output DRD Applied to A Half Table</b>	<b>57</b>
7.1	Output Disturbance Response Decoupling (ODRD) . . . . .	57
7.2	Dynamic Equations . . . . .	59
7.3	Simulation . . . . .	62
7.3.1	Controller Design . . . . .	62
7.3.2	First ODRD . . . . .	63
7.3.3	Second ODRD . . . . .	64
7.3.4	Hybrid ODRD . . . . .	64
<b>8</b>	<b>Input-Output DRD Applied to A Half Table</b>	<b>67</b>
8.1	Input-Output Disturbance Response Decoupling (IODRD) . . . . .	67
8.2	Dynamic Equations . . . . .	69
8.3	Simulation . . . . .	70
8.3.1	Controller Design . . . . .	70
8.3.2	First IODRD . . . . .	71
8.3.3	Second IODRD . . . . .	72
8.3.4	Third IODRD . . . . .	73
8.3.5	Fourth IODRD . . . . .	74
<b>9</b>	<b>Conclusions</b>	<b>77</b>
9.1	Conclusions . . . . .	77
9.2	Future Work . . . . .	78

<b>A</b>	<b>Design of Stabilizing Controller <math>K_1</math></b>	<b>79</b>
A.1	Design of $K_1$ - Quarter Table . . . . .	79
A.2	Design of $K_1$ - Half Table . . . . .	79
A.3	Design of $K_1$ - Full Table . . . . .	80
<b>B</b>	<b>Device Specification</b>	<b>81</b>
	<b>Bibliography</b>	<b>87</b>

# List of Figures

1.1	Linear Fractional Transformation	2
2.1	Vertical Vibration Machine [1]	4
2.2	Compression Spring Ends [2]	5
2.3	Piezo Actuator P-844.20 [3]	6
2.4	Piezoelectric Amplifier E-663 [4]	6
2.5	Voice Coil Motor [5]	7
2.6	Typical Accelerometer Structure Diagram [6].	8
2.7	Accelerometer 731A/P31 [7]	8
2.8	Cutaway View of An LVDT [8].	9
2.9	The transfer function of a typical LVDT [8].	10
2.10	Macro Sensors LVC-2500 [9].	10
2.11	Load Cell [10].	11
2.12	Wheatstone Bridge Configuration [10].	12
2.13	Load Cell MLP-200 [11].	12
3.1	Quarter Table [12]	16
3.2	Bode Plot Of The Quarter Table	18
3.3	Exogenous Disturbances	18
3.4	Outputs of An Open-loop System	19
3.5	Annihilated Outputs	19
3.6	Response of One Piezo Actuator	19
3.7	Regulated Outputs of Open- and Closed-loop System.	20

4.1	Half Table [12]	24
4.2	Bode Plot Of The Half Table	26
4.3	Exogenous Disturbances	27
4.4	Outputs of An Open-loop System	27
4.5	Annihilated Outputs	28
4.6	Response of Piezo Actuators	28
4.7	Regulated Outputs of Open- and Closed-loop System.	29
4.8	Exogenous Disturbances (Limited Piezo Actuators)	30
4.9	Annihilated Outputs (Limited Piezo Actuators)	31
4.10	Response of Piezo Actuators (Limited Piezo Actuators).	31
4.11	Regulated Outputs of Open- and Closed-loop System (Limited Piezo Actuators).	32
5.1	Full Table [12]	37
5.2	Exogenous Disturbances	39
5.3	Outputs of An Open-loop System	40
5.4	Annihilated Outputs	40
5.5	Response of Piezo Actuators	41
5.6	Regulated Outputs of Open- and Closed-loop System.	42
6.1	Open-loop System	44
6.2	General Control Configuration	44
6.3	Closed-loop System	44
6.4	Control Structure of IDR D	50
6.5	Control Structure of IDR D	50
6.6	Control Structure of ODR D	53
6.7	Control Structure of ODR D	54
7.1	Control Structure of ODR D	58
7.2	Half Table [12]	60
7.3	Exogenous Disturbances	62

7.4	Response of Piezo Actuators (1st ODRD). . . . .	63
7.5	Regulated Outputs of Open- and Closed-loop System (1st ODRD). . . . .	63
7.6	Response of Piezo Actuators (2nd ODRD). . . . .	64
7.7	Regulated Outputs of Open- and Closed-loop System (2nd ODRD). . . . .	64
7.8	Response of Piezo Actuators (Hybrid ODRD). . . . .	65
7.9	Regulated Outputs of Open- and Closed-loop System (Hybrid ODRD). . . . .	65
8.1	Control Structure of IODRD . . . . .	68
8.2	Exogenous Disturbances . . . . .	70
8.3	Response of Piezo Actuators (1st IODRD). . . . .	71
8.4	Regulated Outputs of Open- and Closed-loop System (1st IODRD). . . . .	71
8.5	Response of Piezo Actuators (2nd IODRD). . . . .	72
8.6	Regulated Outputs of Open- and Closed-loop System (2nd IODRD). . . . .	72
8.7	Response of Piezo Actuators (3rd IODRD). . . . .	73
8.8	Regulated Outputs of Open- and Closed-loop System (3rd IODRD). . . . .	73
8.9	Response of Piezo Actuators (4th IODRD). . . . .	74
8.10	Regulated Outputs of Open- and Closed-loop System (4th IODRD). . . . .	74



# List of Tables

3.1	Symbol Meanings of The Quarter Table . . . . .	16
3.2	Parameters in The Quarter Table . . . . .	18
3.3	Vibration Reduction of $z_s$ . . . . .	21
3.4	Vibration Reduction of $z_u$ . . . . .	21
4.1	Symbol Meanings of The Half Table . . . . .	25
4.2	Signal Representation of The Half Table . . . . .	25
4.3	Parameters in The Half Table . . . . .	25
4.4	Vibration Reduction of The Regulated Outputs . . . . .	31
4.5	Vibration Reduction of The Regulated Outputs (Limited Piezo Actuators). . . . .	33
5.1	Symbol Meanings of The Full Table . . . . .	37
5.2	Signal Representation of The Full Table . . . . .	37
5.3	Parameters in The Full Table . . . . .	39
5.4	Vibration Reduction of The Regulated Outputs . . . . .	42
7.1	Symbol Meanings of The Half Table . . . . .	61
7.2	Signal Representation of A Simplified Half Table . . . . .	61
7.3	Parameters in The Half Table . . . . .	61
7.4	Vibration Reduction of The Regulated Output $z_s$ . . . . .	66
7.5	Vibration Reduction of The Regulated Output $z_\phi$ . . . . .	66
8.1	Signal Representation of A Simplified Half Table . . . . .	75

8.2	Vibration Reduction of The Regulated Output $z_s$ .	75
8.3	Vibration Reduction of The Regulated Output $z_\phi$ .	75
B.1	Specification of The Vertical Vibration Machine	82
B.2	Specification of P-844.20, Physik Instrumente [3]	82
B.3	Specification of E-663, Physik Instrumente [4]	82
B.4	Specification of AVM35-HF-7, Akribis [13]	83
B.5	Specification of OPA544, Texas Instruments [14]	83
B.6	Specification of Accelerometer 731A/P31, Wilcoxon Research Inc. [7].	83
B.7	Specification of PR 750-050, Macro Sensors [9].	84
B.8	Specification of LVC-2500, Macro Sensors [9].	84
B.9	Specification of MLP-200, Transducer Techniques [11].	84
B.10	Specification of NI PCI-6259 [15].	84
B.11	Specification of NI PCIe-6323 [15].	85

# Abbreviations and Acronyms

LFT	Linear Fractional Transformation
DRD	Disturbance Response Decoupling
IDRD	Input Disturbance Response Decoupling
ODRD	Output Disturbance Response Decoupling
IODRD	Input-Output Disturbance Response Decoupling



# Notation

Symbol	Meaning
$w$	Exogenous disturbance
$z$	Regulated output
$y$	Measured output
$u$	Actuator input
$P$	Generalized plant
$P_{11}$	Sub-plant of the generalized plant $P$
$\hat{P}_{21}$	The Laplace transform of the sub-plant $P_{21}$
$K_1$	A set of stabilizing controller
$K_1^{w_j}$	A stabilizing controller designed for the $j$ -th exogenous disturbance $w_j$
$\tilde{U}_2$	A set of annihilated transfer function
$\tilde{U}_2^{w_j}$	An annihilated transfer function designed for the $j$ -th exogenous disturbance $w_j$
$T_{w_1 \rightarrow z}$	A transfer function from the input $w_1$ to the output $z$



# Chapter 1

## Related Work

### 1.1 Linear Fractional Transformation

Consider a multi-input multi-output (MIMO) system, where  $P$  is the generalized plant model,  $K$  is the controller,  $u$  is the actuator input,  $w$  is the exogenous disturbance,  $z$  is the regulated output,  $y$  is the measured output. The general control configuration can be represented by the following linear fractional transformation (LFT), as shown in Figure 1.1.

$$\begin{pmatrix} z \\ y \end{pmatrix} = \begin{pmatrix} P_{11} & P_{12} \\ P_{21} & P_{22} \end{pmatrix} \begin{pmatrix} w \\ u \end{pmatrix} \quad (1.1)$$

If we take Laplace transform of (1.1), then we have the following form:

$$\begin{pmatrix} \hat{z} \\ \hat{y} \end{pmatrix} = \begin{pmatrix} \hat{P}_{11} & \hat{P}_{12} \\ \hat{P}_{21} & \hat{P}_{22} \end{pmatrix} \begin{pmatrix} \hat{w} \\ \hat{u} \end{pmatrix} \quad (1.2)$$

The generalized plant of (1.2) can be further partitioned into the following form:

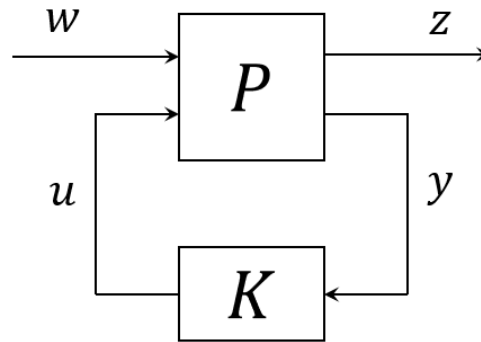


Figure 1.1: Linear Fractional Transformation

$$\begin{pmatrix} \hat{z}_1 \\ \hat{z}_2 \\ \hat{y} \end{pmatrix} = \begin{pmatrix} \hat{P}_{111} & \hat{P}_{112} & \hat{P}_{12} \\ \hat{P}_{211} & \hat{P}_{212} & \hat{P}_{22} \end{pmatrix} \begin{pmatrix} \hat{w}_1 \\ \hat{w}_2 \\ \hat{u} \end{pmatrix} \quad (1.3)$$

In the following chapters, this concept will be applied to a decoupling strategy called disturbance response decoupling (DRD) [16].

# Chapter 2

## Experimental Setup

### 2.1 Components in An Optical Table

#### 2.1.1 Vertical Vibration Machine

The disturbance  $z_r$  in my experiment is generated by a vertical vibration machine. A ball screw servo motor is installed inside the machine to transform the motor axial rotation to an axial movement. This axial movement represents the disturbance  $z_r$ . For details, please refer to [Figure 2.1](#) and [Table B.1](#).

#### 2.1.2 Linear Spring

The spring comes in varieties – the compression spring, the extension spring, the torsion spring, etc. – all of which serve different and specific functions. For compression springs there are two basic end type options – closed or open, with both options having either ground or not ground ends, as shown in [Figure 2.2](#). Closed and ground compression springs are the most common and sit the most flat because grinding process is applied to the ends of this kind of springs. Thus closed and ground compression springs are chosen as my components in my experiment, and the spring constant can be calculated from the dimensions of the compression springs:

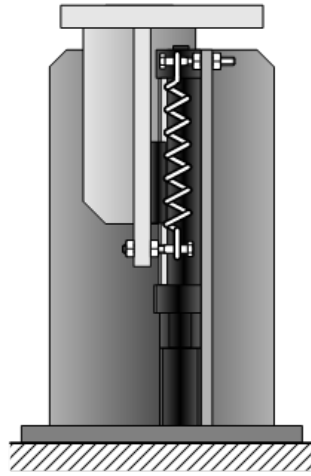


Figure 2.1: Vertical Vibration Machine [1]

$$k = \frac{Gd^4}{8nD^3} \quad (2.1)$$

where  $G$  is transverse elastic modulus ( $N/mm^2$ ),  $d$  is material diameter (mm),  $n$  is number of active coils,  $D$  is coil mean diameter.

Hooke's law, discovered by the English scientist Robert Hooke in 1660, states that, for relatively small deformations of an object, the displacement or size of the deformation is directly proportional to the deforming force or load. Hooke's law can be formulated as:

$$F = -kx \quad (2.2)$$

where  $k$  is the spring constant,  $F$  is the force, and  $x$  is the length of extension/compression.

In the real world, however, springs are influenced by restoring forces and friction, and frictional forces will diminish the amplitude of oscillation until eventually the system is at rest. To make the entire model closer to the real model, springs can be modelled as:

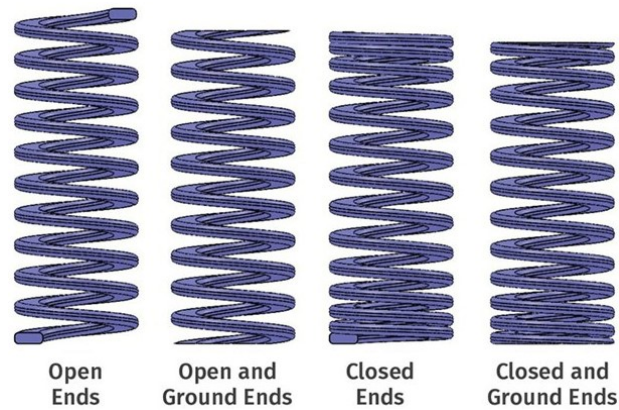


Figure 2.2: Compression Spring Ends [2]

$$\theta = cs + k \quad (2.3)$$

where  $\theta$  is the damped spring model in Laplace domain,  $c$  is damping ratio of the spring, and  $k$  is the spring constant.

### 2.1.3 Piezoelectric Actuator

The optical-table model needs active linear actuator to reduce the vibration from the disturbances. Because high resolution of the actuator is required, Physik Instrumente (PI) offers one kind of piezo actuator: P-844.20 ( Figure 2.3). For details about P-844.20, please refer to Table B.2.

Besides, the voltage input of the selected piezo actuators should be amplified, so a piezo amplifier is required. The PI E-663 amplifier in Figure 2.4 has three low-noise amplifier channels for low-volt piezo actuators that input and output peak currents of 140 mA in a voltage range of -20 to +120 V. For details, please refer to Table B.3.



Figure 2.3: Piezo Actuator P-844.20 [3]



Figure 2.4: Piezoelectric Amplifier E-663 [4]

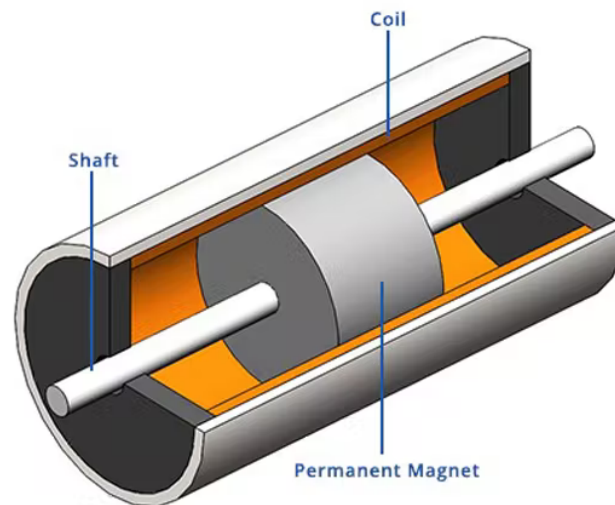


Figure 2.5: Voice Coil Motor [5]

### 2.1.4 Voice Coil Motor

A voice coil motor (VCM) is used to generate the force  $F_s$  on top of the mass  $m_s$ . The VCM consists of a permanent magnetic field assembly and a coil assembly, as shown in Figure 2.5. The current flowing through the coil assembly interacts with the permanent magnetic field and generates a force by Lorentz' force equation. The VCM are is commonly used for short travel paths where high acceleration and constant force is required, and Akribis's VCM AVM35-HF-7 meets our requirement. For details, please refer to Table B.4.

Besides, Texas Instruments has a high-voltage/high-current operational amplifier (OPA544) suitable for driving VCM. For details, please refer to Table B.5.

### 2.1.5 Accelerometer

An accelerometer is a device that measures the acceleration of a structure. As shown in Figure 2.6, an accelerometer comprises a spring, a seismic mass, and a displacement sensor arranged within a housing attached to a base. The relative displacement between the seismic mass and the base can be recorded by the

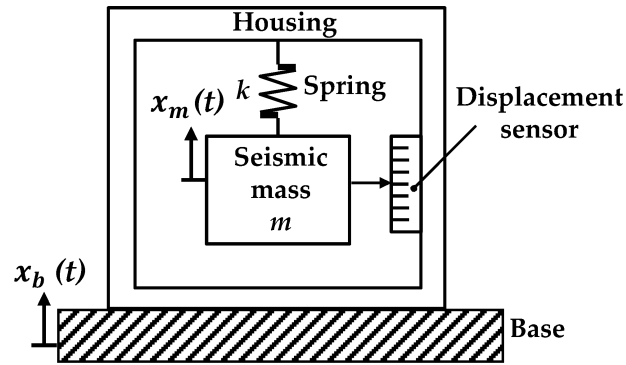


Figure 2.6: Typical Accelerometer Structure Diagram [6].



Figure 2.7: Accelerometer 731A/P31 [7]

displacement sensor expressed as [6]:

$$x_m - x_b = \frac{m}{k} a \quad (2.4)$$

where  $x_m$  is the displacement of the seismic mass,  $x_b$  is the displacement of the base,  $m$  is the seismic mass,  $k$  is the spring constant, and  $a$  is the acceleration we want to know.

Wilcoxon Sensing Technologies® produces ultra-low frequency seismic accelerometers 731A/P31 Figure 2.7, which can measure the acceleration of my system. For details, please refer to Table B.6.

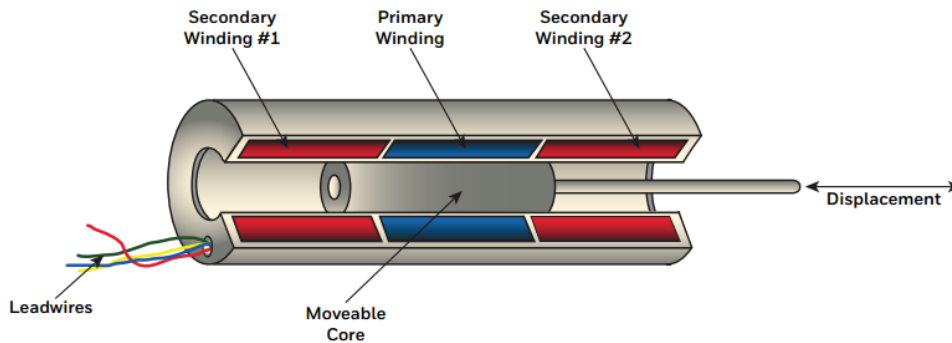


Figure 2.8: Cutaway View of An LVDT [8].

### 2.1.6 Linear Variable Differential Transformer

The linear variable differential transformer (LVDT), as shown in Figure 2.8, is a contactless linear position sensor converting the rectilinear motion of an object into a corresponding electrical signal. Friction-free operation, high resolution (infinite in theory), high linearity (0.5% or better), and high sensitivity are some of the important features of the LVDT devices.

Figure 2.9 shows the transfer function of a typical LVDT. The x-axis is the core displacement from the center. The y-axis is the amplitude of the output AC voltage. At the origin ( $x = 0$ ), the output is ideally zero. As the core is moved off center in either direction, the amplitude of the output increases linearly with the core displacement. This, LVDT has high linearity in the linear range.

To measure some displacements, such as  $z_s$  and  $z_u$  in my experiment, PR 750 LVDTs offered by Macro Sensors are the suitable sensors. Also, to support this LVDT sensors, we connect a single channel signal conditioner, Macro Sensors LVC-2500 ( Figure 2.10), that operates on 10-30 Volts DC power. For details, please refer to specification of LVDTs Table B.7 and the corresponding amplifier Table B.8.

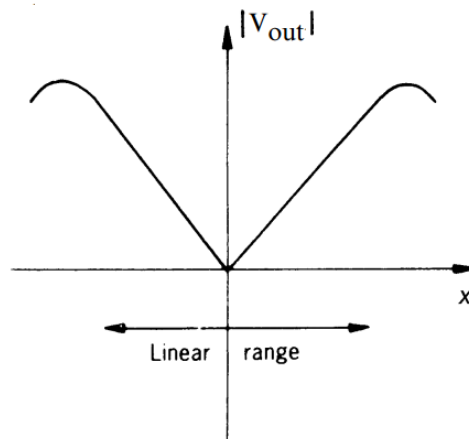


Figure 2.9: The transfer function of a typical LVDT [8].



Figure 2.10: Macro Sensors LVC-2500 [9].

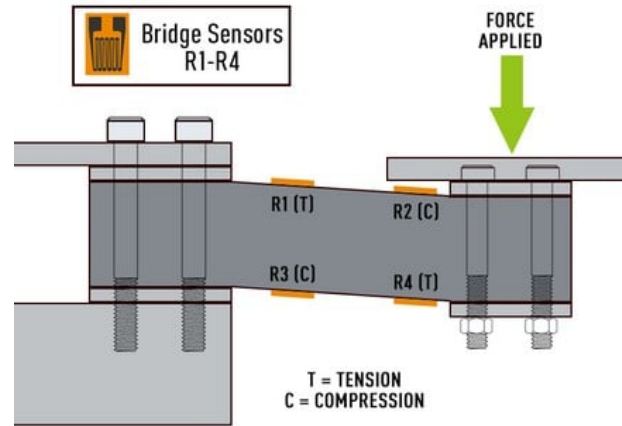


Figure 2.11: Load Cell [10].

### 2.1.7 Load Cell

Load cell is a force sensor that converts a load or force acting on it into an electrical signal. One kind of load cells, strain gauge load cell as shown in Figure 2.11, works on the principle of changing electrical resistance as the conductor is being elastically deformed, and multiple strain gauges are used to set in a Wheatstone bridge configuration (balanced when no load is applied, shown in Figure 2.12) in order to achieve a very high degree of accuracy. The overall change in resistance across all four strain gauges can be determined by using Ohm's law [10]:

$$v_O = \left[ \frac{R_3}{R_3 + R_4} - \frac{R_2}{R_1 + R_2} \right] v_{EX} \quad (2.5)$$

where  $v_O$  is the output voltage, and  $v_{EX}$  is the voltage excitation.

To measure some forces, such as  $F_s$  in my experiment, Transducer Techniques MLP-200 is a suitable force sensor, as shown in Figure 2.13. For details, please refer to Table B.9.

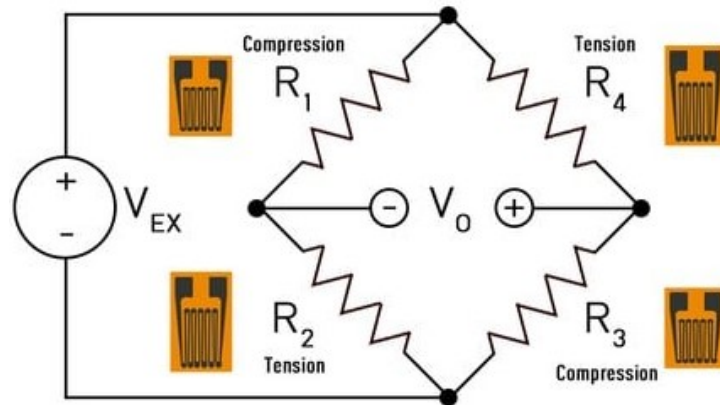


Figure 2.12: Wheatstone Bridge Configuration [10].



Figure 2.13: Load Cell MLP-200 [11].

### **2.1.8 Multifunction I/O Device**

The National Instruments (NI) multifunction I/O device offers analog I/O, correlated digital I/O, 32-bit counters/timers, and analog and digital triggering. The device delivers low-cost, reliable DAQ capabilities in a wide range of applications from simple applications in laboratory automation, research, design verification/test, and manufacturing test. All sensors we used in the experiment are added to this NI device. For details, please refer to [Table B.10](#) and [Table B.11](#).



# Chapter 3

## Quarter Table

### 3.1 Dynamics Equations

A quarter-table model is used to study the dynamics of an optical table [1, 17]. Figure 3.1 illustrates the free body diagram, and its corresponding equations of motion can be derived as:

$$m_s \ddot{z}_s = F_s - \theta_2(z_s - z_u) - \theta_3(z_a - z_u) \quad (3.1)$$

$$m_u \ddot{z}_u = \theta_2(z_s - z_u) + \theta_3(z_a - z_u) - \theta_1(z_u - z_r) \quad (3.2)$$

where each parameter is defined in Table 3.1. And the displacement output of  $z_a$  can be substituted by the transfer function  $\gamma$ :

$$z_a - z_s = \gamma u \quad (3.3)$$

Then, the equation (3.1), (3.2), and (3.3) can be formulated into LFT form in (1.3), where the exogenous disturbance  $w$  is  $[z_r, F_s]^T$ , the regulated output  $z$  is  $[z_s, z_u]^T$ , the measured output  $y$  is  $[z_s, z_u]^T$ . The actuator input  $u$  is a scalar because only one piezo actuator is used in the case the quarter table.

Table 3.1: Symbol Meanings of The Quarter Table

Symbol	Meaning
$m_s$	Sprung mass
$m_u$	Unsprung mass
$F_s$	Force applying on the sprung mass
$\theta_1$	A passive component connecting $m_u$ and the platform
$\theta_2$	A passive component connecting $m_u$ and $m_s$
$\theta_3$	A passive component connecting $m_u$ and the piezo actuator
$z_s$	Displacement of the sprung mass
$z_u$	Displacement of the unsprung mass
$z_r$	Displacement of the platform
$z_a$	Displacement output of the piezo actuator
$\gamma$	Transfer function from input voltage to the displacement ( $z_a - z_s$ )

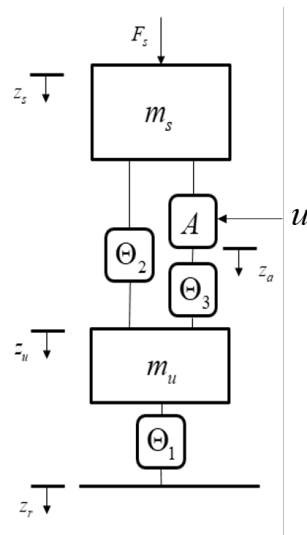


Figure 3.1: Quarter Table [12]

## 3.2 Controller Design

### 3.2.1 Design of $\tilde{U}_2$

The annihilated output  $\tilde{U}_2$  can be calculated from the inverse of  $\hat{P}_{21}$  in (1.2).

### 3.2.2 Design of $K_1$

The stabilizing controller  $K_1$  is constructed by MATLAB `ncfsyn` function, and  $K_1^{w_1}$  and  $K_1^{w_2}$  are shown in Appendix (A.1) and (A.2).

## 3.3 Simulation

After LFT form of the equations of motion is derived, the numerical model can be calculated by substituting all values in Table 3.2. Note that the passive components  $\theta_j$  is the combination of a linear spring  $k_j$  and a damper  $c_j$ , where  $j = 1, 2, 3$ . Then we can generate two disturbances to simulate the vibrational situation. The disturbances  $w$  are given in equation (3.4) (3.5) and also shown in Figure 3.3. I plot the frequency response of the open-loop system and find that the transfer function  $T_{u \rightarrow z_r}$  and  $T_{u \rightarrow F_s}$  in bode plot (shown in Figure 3.2) has maximum values at around 12 and 13 Hz. Therefore, 12 and 13 Hz are chosen as the frequencies of two disturbance signals.

$$\begin{cases} z_r = 0.0002 \sin(26\pi t) & (\text{unit} : m) & (3.4) \\ F_s = 20 \sin(24\pi t) & (\text{unit} : N) & (3.5) \end{cases}$$

First, we observe the open-loop system of the quarter table, as shown in Figure 3.4.

The closed-loop system constructed by designing  $\tilde{U}_2^{w_1}$ ,  $\tilde{U}_2^{w_2}$ ,  $K_1^{w_1}$ , and  $K_1^{w_2}$  has the following corresponding annihilated outputs  $\tilde{y}^{w_1}$ ,  $\tilde{y}^{w_2}$ , as shown in Figure 3.5.

Also, because the purpose of the piezo actuator is to reduce the exogenous signal  $w$ , its output response matters in my simulation, as shown in Figure 3.6.

Table 3.2: Parameters in The Quarter Table

Symbol	Value	Unit
$m_s$	19.0322	kg
$m_u$	11.5250	kg
$c_1$	373.558	Ns/m
$c_2$	289.247	Ns/m
$c_3$	446.353	Ns/m
$k_1$	$2.43584 \times 10^5$	N/m
$k_2$	$2.02263 \times 10^5$	N/m
$k_3$	$5.81508 \times 10^5$	N/m
$\gamma$	$\frac{0.0005662}{s+272.2}$	

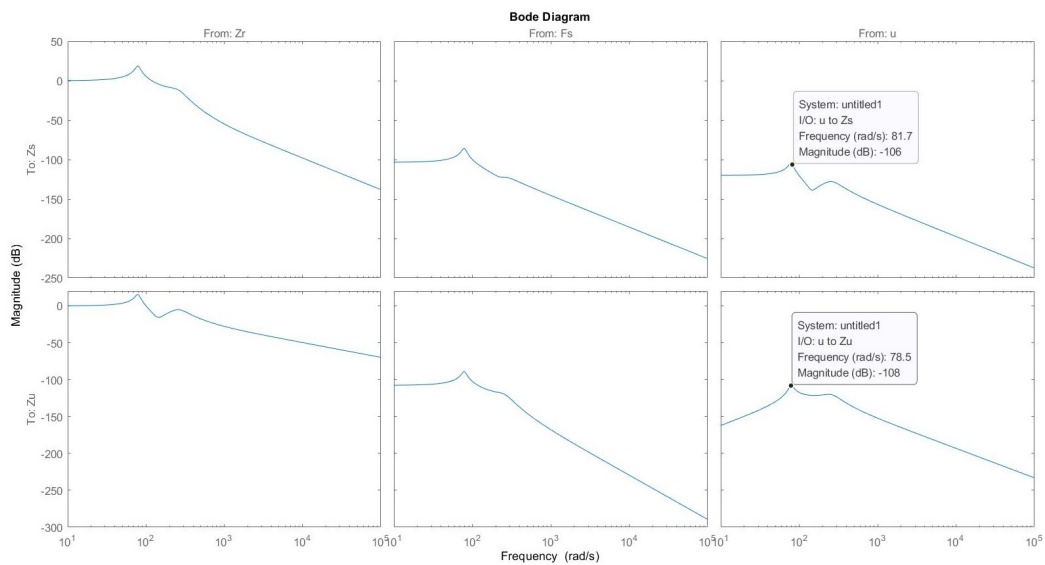


Figure 3.2: Bode Plot Of The Quarter Table

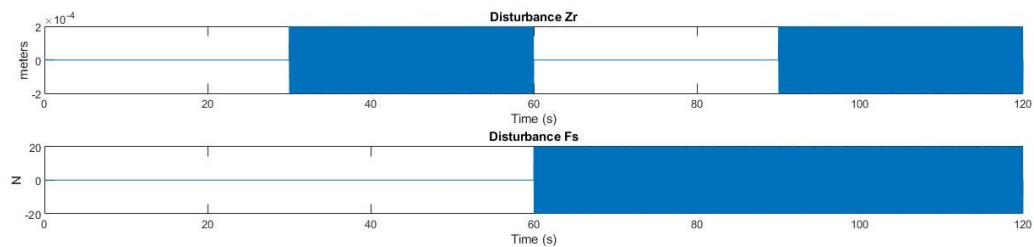


Figure 3.3: Exogenous Disturbances

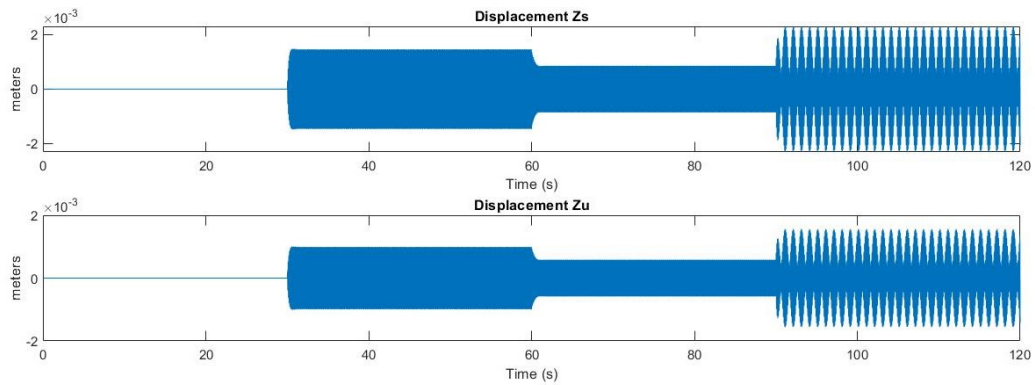


Figure 3.4: Outputs of An Open-loop System

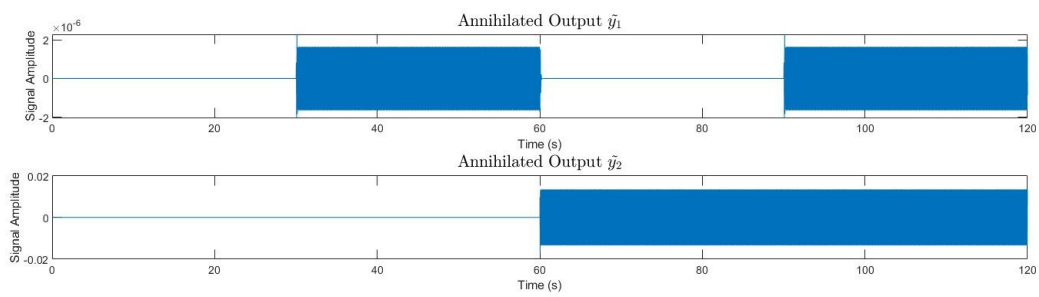


Figure 3.5: Annihilated Outputs

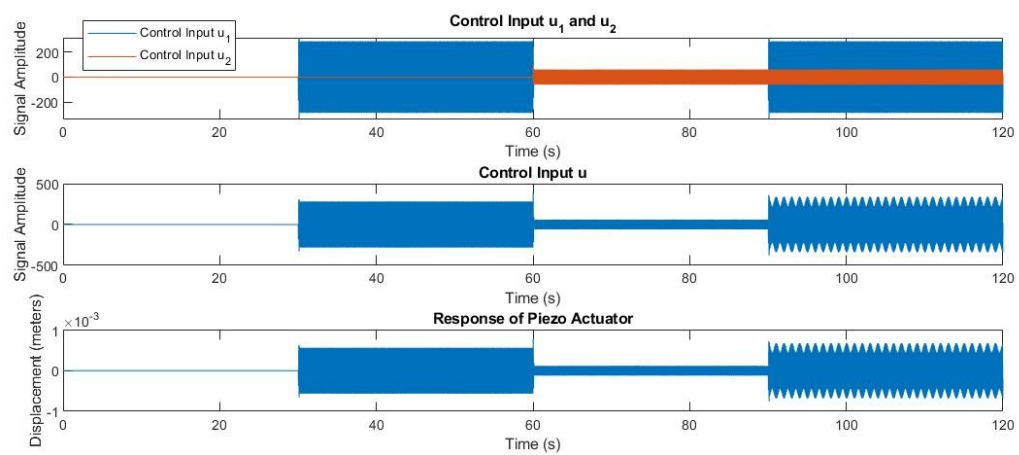


Figure 3.6: Response of One Piezo Actuator

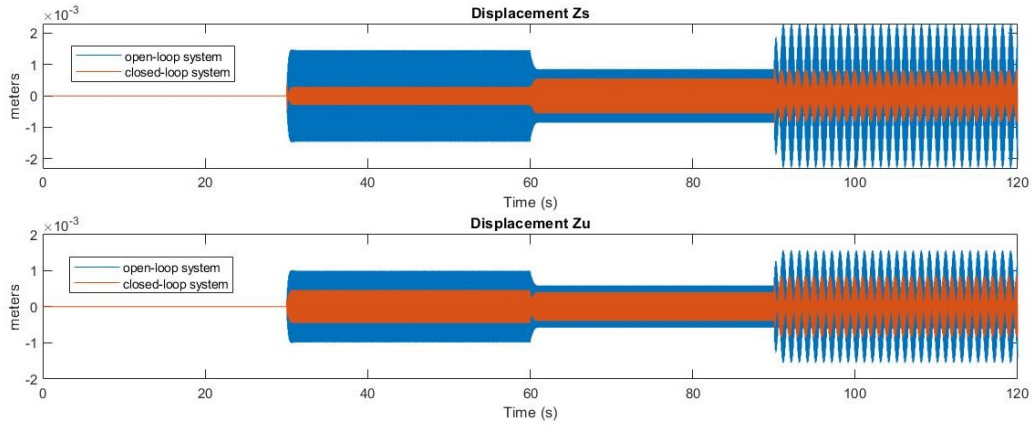


Figure 3.7: Regulated Outputs of Open- and Closed-loop System.

In my simulation, the maximum amplitude of  $(z_a - z_s)$  is approximately 550  $\mu\text{m}$ .

### 3.3.1 Vibration Reduction

The importance of my research is to reduce the regulated outputs  $z = [z_s, z_u]^T$ , so, here, I compare the open-loop and closed-loop system in Figure 3.7.

For the duration from 100 to 120 seconds, the vibration reduction is significant when both controllers are open.

Table 3.3: Vibration Reduction of  $z_s$ 

	$K_1^{w_1}$ off	$K_1^{w_1}$ open
$K_1^{w_2}$ off	NA	46.7%
$K_1^{w_2}$ open	7.66%	63.0%

Table 3.4: Vibration Reduction of  $z_u$ 

	$K_1^{w_1}$ off	$K_1^{w_1}$ open
$K_1^{w_2}$ off	NA	35.5%
$K_1^{w_2}$ open	7.08%	47.2%



# Chapter 4

## Half Table

### 4.1 Dynamics Equations

A half-table model is used to study the dynamics of an optical table [1, 17]. Figure 7.2 illustrates the free body diagram, and its corresponding equations of motion can be derived as:

$$m_s \ddot{z}_s = F_s - u_{p1} - u_{p2} \quad (4.1)$$

$$I_\phi \ddot{z}_\phi = T_\phi - u_{p1} l_1 + u_{p2} l_2 \quad (4.2)$$

$$m_{u1} \ddot{z}_{u1} = u_{p1} - \theta_{11} (z_{u1} - z_{r1}) \quad (4.3)$$

$$m_{u2} \ddot{z}_{u2} = u_{p2} - \theta_{12} (z_{u2} - z_{r2}) \quad (4.4)$$

where  $u_{p1}$  and  $u_{p2}$  are defined as:

$$u_{p1} = \theta_{21} (z_s + l_1 z_\phi - z_{u1}) + \theta_{31} (z_{a1} - z_{u1}) \quad (4.5)$$

$$u_{p2} = \theta_{22} (z_s - l_2 z_\phi - z_{u2}) + \theta_{32} (z_{a2} - z_{u2}) \quad (4.6)$$

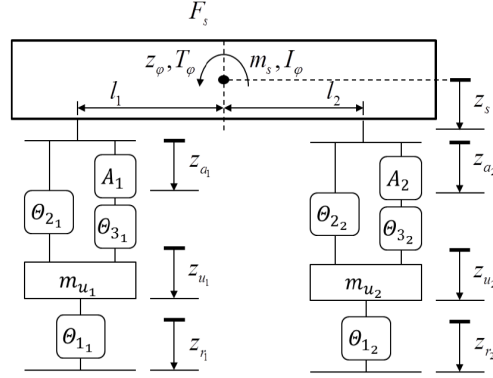


Figure 4.1: Half Table [12]

where each parameter is defined in Table 7.1. And the displacement output of  $z_a$  can be substituted by the transfer function  $\gamma$ :

$$z_{a_1} - z_s - l_1 z_\phi = \gamma u_1 \quad (4.7)$$

$$z_{a_2} - z_s + l_2 z_\phi = \gamma u_2 \quad (4.8)$$

Then, the above equations can be formulated into LFT form described in (1.3), where the signals  $w, z, u, y$  are defined in Table 4.2.

## 4.2 Controller Design

### 4.2.1 Design of $\tilde{U}_2$

The annihilated output  $\tilde{U}_2$  can be calculated from the inverse of  $\hat{P}_{21}$  in (1.2).

### 4.2.2 Design of $K_1$

The stabilizing controller  $K_1$  is constructed by MATLAB `ncfsyn` function, and  $K_1^{w_1}, K_1^{w_2}, K_1^{w_3}$  and  $K_1^{w_4}$  are shown in Appendix from (A.3) to (A.6).

Table 4.1: Symbol Meanings of The Half Table

Symbol	Meaning
$m_s$	Sprung mass
$m_u$	Unsprung mass
$F_s$	Force applying on the sprung mass
$\theta_{1j}$	A passive component connecting $m_u$ and the platform, where $j = 1, 2$
$\theta_{2j}$	A passive component connecting $m_u$ and $m_s$ , where $j = 1, 2$
$\theta_{3j}$	A passive component connecting $m_u$ and the piezo actuator, where $j = 1, 2$
$z_s$	Displacement of the sprung mass
$z_{u_j}$	Displacement of the unsprung mass, where $j = 1, 2$
$z_{r_j}$	Displacement of the platform, where $j = 1, 2$
$z_{a_j}$	Displacement output of the piezo actuator, where $j = 1, 2$
$\gamma_j$	Transfer function from input voltage to the displacement ( $z_{a_j} - z_s$ )

Table 4.2: Signal Representation of The Half Table

Symbol	Signal Representation
Exogenous disturbance $w$	$[z_{r_1}, z_{r_2}, F_s, T_\phi]^T$
Regulated output $z$	$[z_s, z_\phi, z_{u_1}, z_{u_2}]^T$
Actuator input $u$	$[u_1, u_2]^T$
Measured output $y$	$[z_s, z_\phi, z_{u_1}, z_{u_2}]^T$

Table 4.3: Parameters in The Half Table

Symbol	Value	Unit
$m_s$	10.8090	kg
$m_{u_1}$	9.451	kg
$m_{u_2}$	12.630	kg
$c_{1j}$	373.558	Ns/m
$c_{2j}$	289.247	Ns/m
$c_{3j}$	446.353	Ns/m
$k_{1j}$	$2.435\ 84 \times 10^5$	N/m
$k_{2j}$	$2.022\ 63 \times 10^5$	N/m
$k_{3j}$	$5.815\ 08 \times 10^5$	N/m
$l_1$	0.225	m
$l_2$	0.225	m
$\gamma$	$\frac{0.0005662}{s+272.2}$	

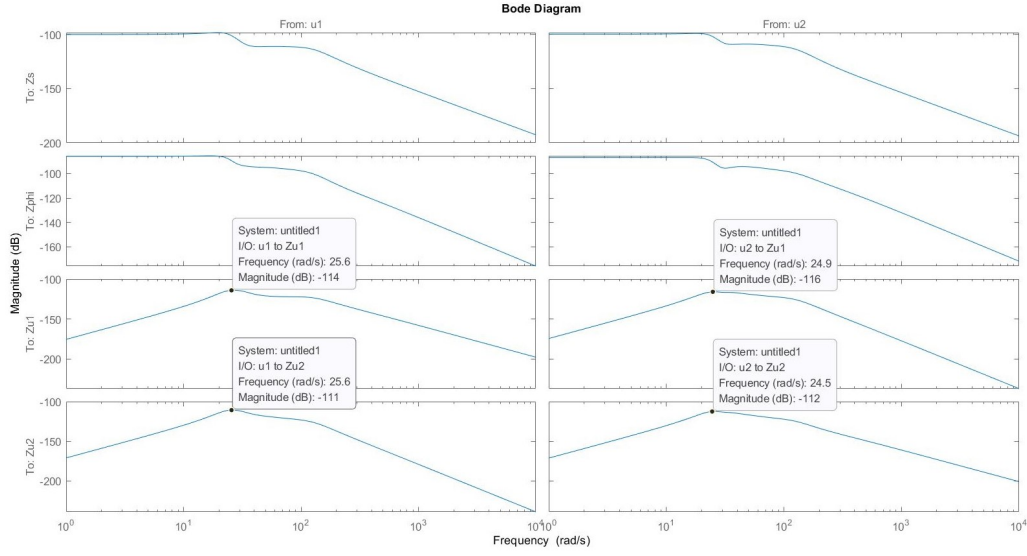


Figure 4.2: Bode Plot Of The Half Table

### 4.3 Simulation - Maximize The Vibration Reduction without Constrained Stroke of Piezo Actuator

Note: We assume that the output of PZT is unlimited in this section.

After LFT form of the equations of motion is derived, the numerical model can be calculated by substituting all values in Table 7.3. Then we can generate some disturbances to simulate the vibrational situation. The disturbances  $w$  are given in equation (4.9), (4.10), (4.11) and (4.12) and also shown in Figure 4.3.

$$\begin{cases} z_{r1} = 0.0001 \sin(4.10\pi t) & (\text{unit : } m) & (4.9) \end{cases}$$

$$\begin{cases} z_{r2} = 0.0001 \sin(6.72\pi t) & (\text{unit : } m) & (4.10) \end{cases}$$

$$\begin{cases} F_s = 10 \sin(9.04\pi t) & (\text{unit : } N) & (4.11) \end{cases}$$

$$\begin{cases} T_\phi = \sin(5.90\pi t) & (\text{unit : } N * m) & (4.12) \end{cases}$$

First, we observe the open-loop system of the half table, as shown in Figure 4.4.

### 4.3. Simulation - Maximize The Vibration Reduction without Constrained Stroke of Piezo Actuator<sup>27</sup>

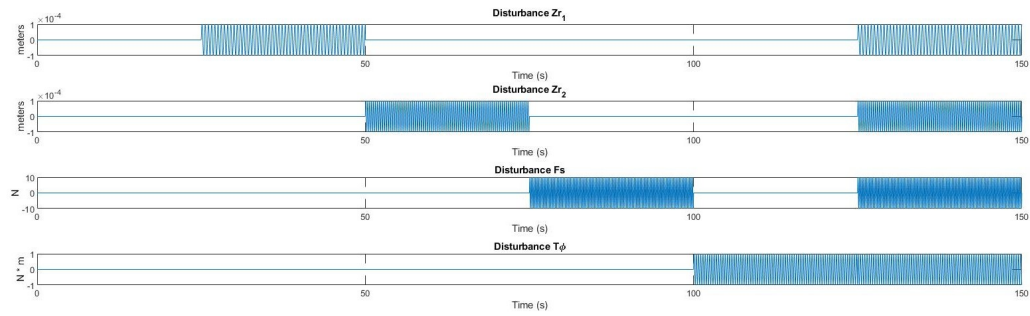


Figure 4.3: Exogenous Disturbances

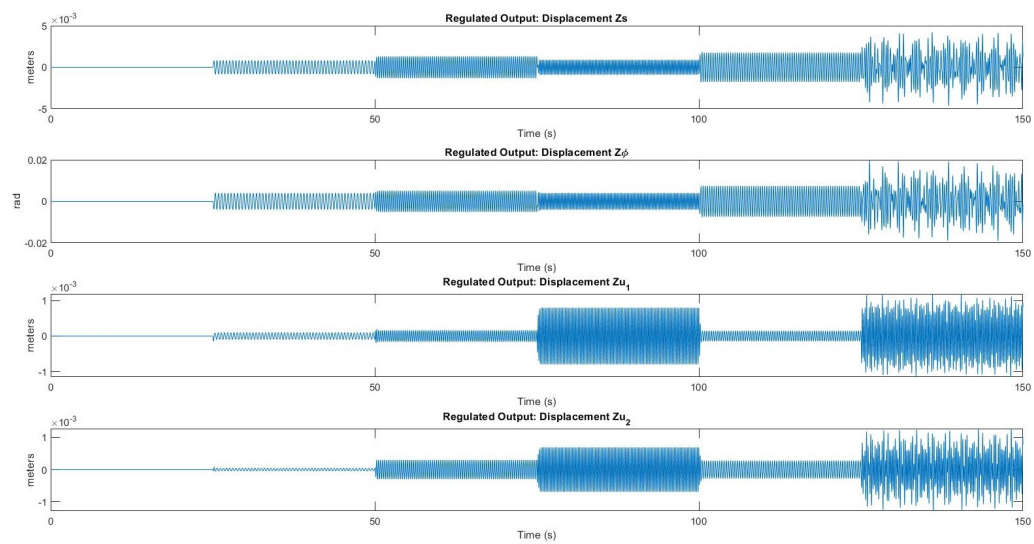


Figure 4.4: Outputs of An Open-loop System

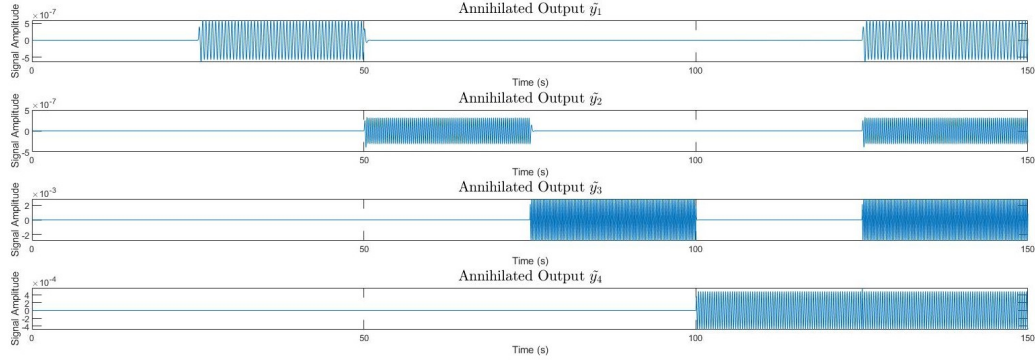


Figure 4.5: Annihilated Outputs

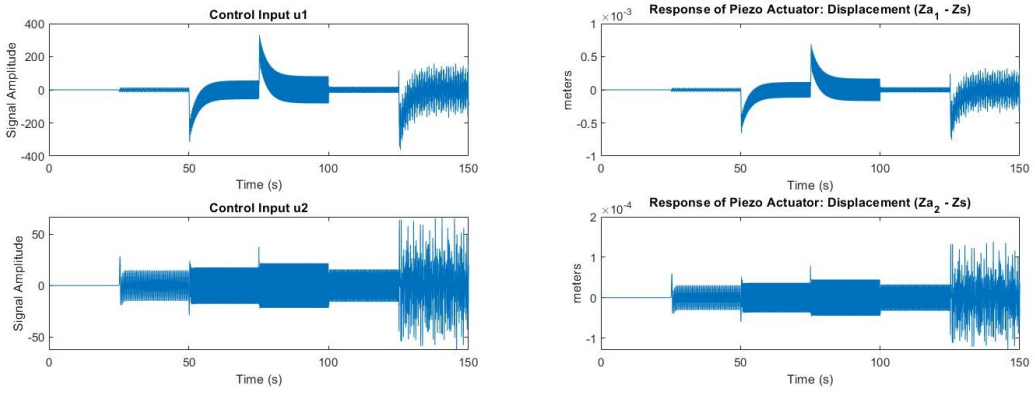


Figure 4.6: Response of Piezo Actuators

The closed-loop system constructed by designing  $\tilde{U}_2^{w_i}$ , and  $K_1^{w_i}$ , where  $i = 1, 2, 3, 4$ , has the following corresponding annihilated outputs  $\tilde{y}^{w_i}$ , as shown in Figure 4.9.

Also, because the purpose of the piezo actuator is to reduce the exogenous signal  $w$ , its output response matters in my simulation, as shown in Figure 4.10.

In my simulation, if only the steady state is considered, it can be observed that the maximum amplitude of  $(z_a - z_s)$  is approximately 330 and 135  $\mu\text{m}$  for the first and second piezo actuator, respectively.

#### 4.4. Simulation - Maximize The Vibration Reduction with Limited Stroke of Piezo Actuator 29

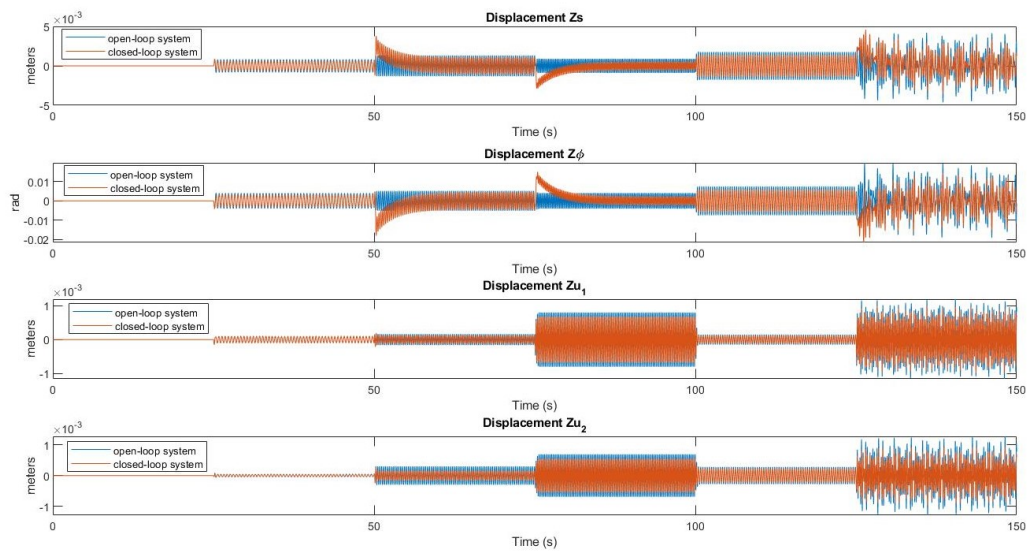


Figure 4.7: Regulated Outputs of Open- and Closed-loop System.

### 4.3.1 Vibration Reduction

The importance of my research is to reduce the regulated outputs  $z$ , so, here, I compare the open-loop and closed-loop system in Figure 4.7.

For the duration from 130 to 150 seconds, the vibration reduction is significant when four controllers are open. See Table 4.4 for more details.

## 4.4 Simulation - Maximize The Vibration Reduction with Limited Stroke of Piezo Actuator

Note: The output of PZT in this section is limited.

After LFT form of the equations of motion is derived, the numerical model can be calculated by substituting all values in Table 7.3. Then we can generate some disturbances to simulate the vibrational situation. The disturbances  $w$  are given in equation from (4.13) to (4.16) and also shown in Figure 4.8.

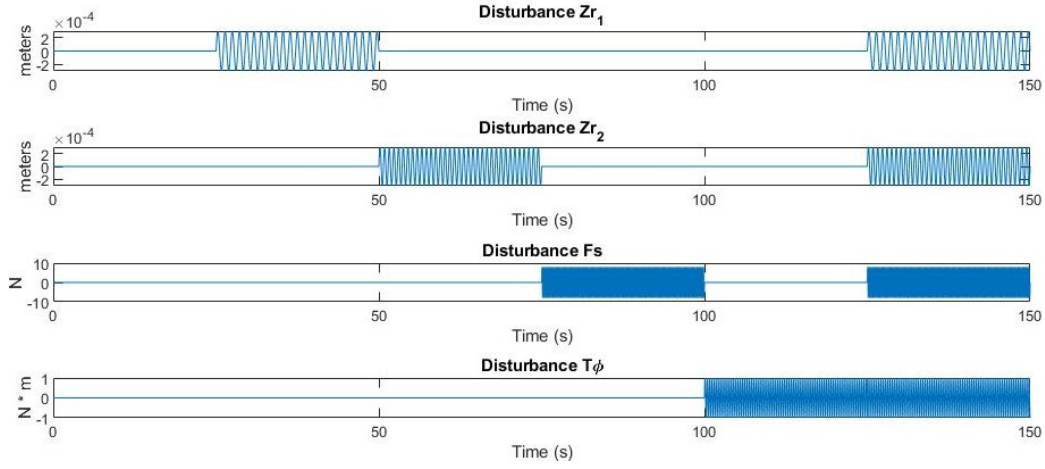


Figure 4.8: Exogenous Disturbances (Limited Piezo Actuators)

$$\begin{cases} z_{r1} = 0.0003 \sin(1.8\pi t) & (\text{unit} : m) & (4.13) \\ z_{r2} = 0.0003 \sin(2.8\pi t) & (\text{unit} : m) & (4.14) \\ F_s = 8 \sin(10.0\pi t) & (\text{unit} : N) & (4.15) \\ T_\phi = \sin(5.90\pi t) & (\text{unit} : N * m) & (4.16) \end{cases}$$

The closed-loop system constructed by designing  $\tilde{U}_2^{w_i}$ , and  $K_1^{w_i}$ , where  $i = 1, 2, 3, 4$ , has the following corresponding annihilated outputs  $\tilde{y}^{w_i}$ , as shown in Figure 4.9.

Also, because the purpose of the piezo actuator is to reduce the exogenous signal  $w$ , its output response matters in my simulation, as shown in Figure 4.10.

In my simulation, if only the steady state is considered, it can be observed that the maximum amplitude of  $(z_a - z_s)$  is approximately 123 and 144  $\mu\text{m}$  for the first and second piezo actuator, respectively.

#### 4.4.1 Vibration Reduction

The importance of my research is to reduce the regulated outputs  $z$ , so, here, I compare the open-loop and closed-loop system in Figure 4.11.

#### 4.4. Simulation - Maximize The Vibration Reduction with Limited Stroke of Piezo Actuator31

Table 4.4: Vibration Reduction of The Regulated Outputs

	$z_s$	$z_\phi$	$z_{u_1}$	$z_{u_2}$
only $K_1^{w_1}$ open	2.15%	2.52%	-0.04%	0.06%
only $K_1^{w_2}$ open	4.80%	2.30%	0.85%	5.17%
only $K_1^{w_3}$ open	4.08%	4.97%	14.1%	15.3%
only $K_1^{w_4}$ open	10.2%	10.2%	0.44%	1.90%
All $K_1^{w_i}$ open ( $i = 1, 2, 3, 4$ )	23.0%	21.5%	15.6%	24.0%

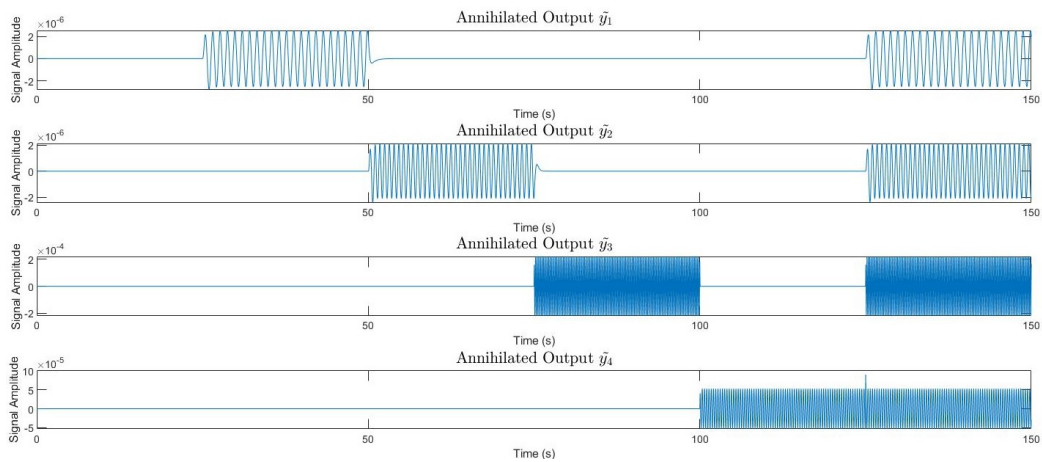


Figure 4.9: Annihilated Outputs (Limited Piezo Actuators)

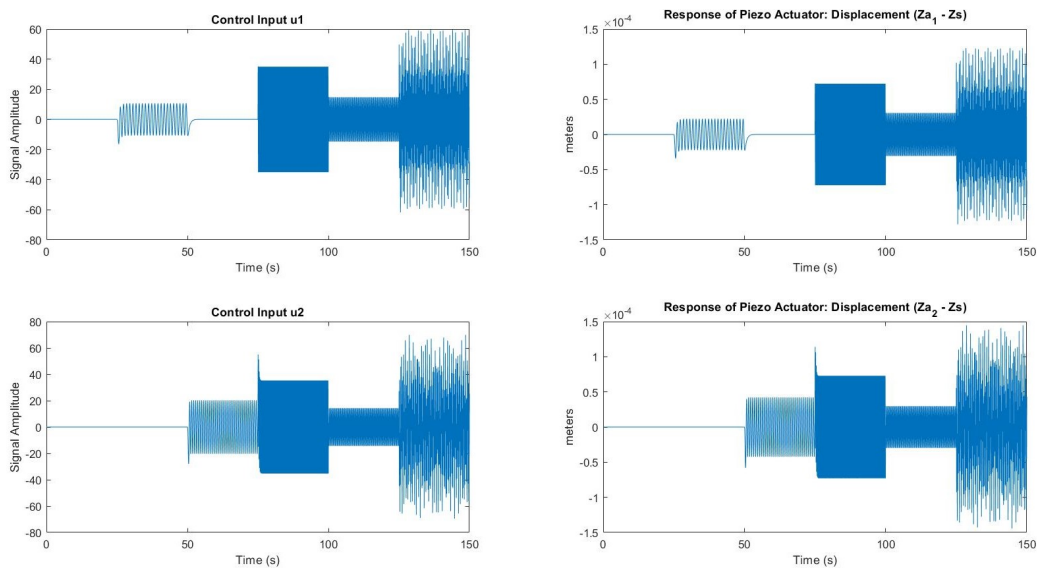


Figure 4.10: Response of Piezo Actuators (Limited Piezo Actuators).

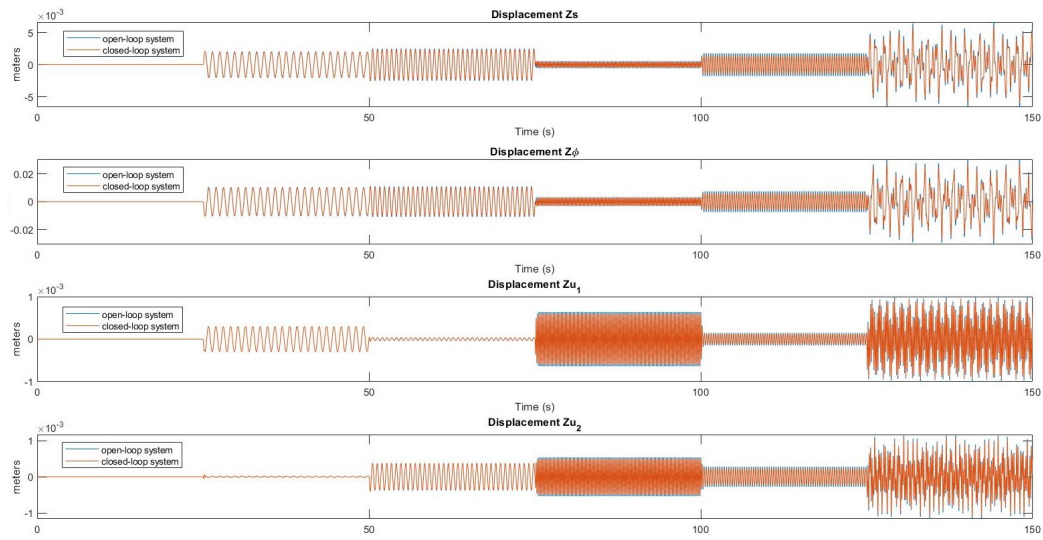


Figure 4.11: Regulated Outputs of Open- and Closed-loop System (Limited Piezo Actuators).

For the duration from 130 to 150 seconds, the vibration reduction is significant when four controllers are open. See Table 4.5 for more details.

#### 4.4. Simulation - Maximize The Vibration Reduction with Limited Stroke of Piezo Actuator33

Table 4.5: Vibration Reduction of The Regulated Outputs (Limited Piezo Actuators).

	$z_s$	$z_\phi$	$z_{u_1}$	$z_{u_2}$
only $K_1^{w_1}$ open	0.92%	1.13%	-0.03%	0.00%
only $K_1^{w_2}$ open	2.65%	2.39%	0.01%	0.32%
only $K_1^{w_3}$ open	0.32%	0.27%	5.45%	4.08%
only $K_1^{w_4}$ open	3.94%	3.30%	0.49%	2.19%
All $K_1^{w_i}$ open ( $i = 1, 2, 3, 4$ )	8.03%	7.27%	5.96%	6.71%



# Chapter 5

## Full Table

### 5.1 Dynamics Equations

A full-table model is used to study the dynamics of an optical table [1, 17]. Figure 5.1 illustrates the free body diagram, and its corresponding equations of motion can be derived as:

$$m_s \ddot{z}_s = F_s - u_{p_1} - u_{p_2} - u_{p_3} - u_{p_4} \quad (5.1)$$

$$I_\theta \ddot{\theta} = T_\theta + u_{p_1} l_f + u_{p_2} l_f - u_{p_3} l_r - u_{p_4} l_r \quad (5.2)$$

$$I_\phi \ddot{\phi} = T_\phi - u_{p_1} t_f + u_{p_2} t_f - u_{p_3} t_r + u_{p_4} t_r \quad (5.3)$$

$$m_{u_1} \ddot{z}_{u_1} = u_{p_1} - F_{r_1} \quad (5.4)$$

$$m_{u_2} \ddot{z}_{u_2} = u_{p_2} - F_{r_2} \quad (5.5)$$

$$m_{u_3} \ddot{z}_{u_3} = u_{p_3} - F_{r_3} \quad (5.6)$$

$$m_{u_4}\ddot{z}_{u_4} = u_{p_4} - F_{r_4} \quad (5.7)$$

where  $u_{p_j}$ ,  $F_{r_j}$ , and  $D_j$  ( $j = 1, 2, 3, 4$ ) are defined as:

$$u_{p_j} = \theta_{2_j}D_j + \theta_{3_j}(z_{a_j} - z_{u_j}) \quad (5.8)$$

$$F_{r_j} = \theta_{1_j}(z_{u_j} - z_{r_j}) \quad (5.9)$$

$$D_1 = z_s - l_f z_\theta + t_f z_\phi - z_{u_1} \quad (5.10)$$

$$D_2 = z_s - l_f z_\theta - t_f z_\phi - z_{u_2} \quad (5.11)$$

$$D_3 = z_s + l_r z_\theta + t_r z_\phi - z_{u_3} \quad (5.12)$$

$$D_4 = z_s + l_r z_\theta - t_r z_\phi - z_{u_4} \quad (5.13)$$

where each parameter is defined in Table 5.1. And the displacement output of  $z_{a_j}$  can be substituted by the transfer function  $\gamma$ :

$$z_{a_1} - z_s + l_f z_\theta - t_f z_\phi = \gamma u_1 \quad (5.14)$$

$$z_{a_2} - z_s + l_f z_\theta + t_f z_\phi = \gamma u_2 \quad (5.15)$$

$$z_{a_3} - z_s - l_r z_\theta - t_r z_\phi = \gamma u_3 \quad (5.16)$$

$$z_{a_4} - z_s - l_r z_\theta + t_r z_\phi = \gamma u_4 \quad (5.17)$$

Then, the above equations can be formulated into LFT form described in (1.3), where the signals  $w, z, u, y$  are defined in Table 5.2.

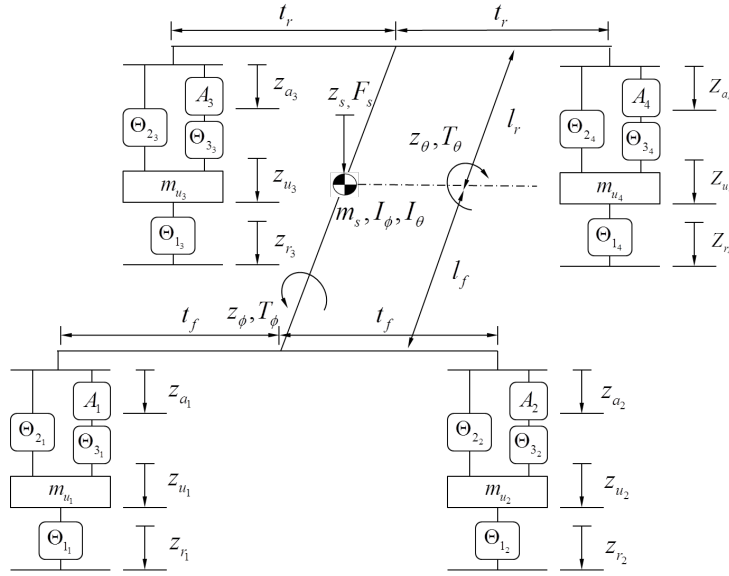


Figure 5.1: Full Table [12]

Table 5.1: Symbol Meanings of The Full Table

Symbol	Meaning
$m_s$	Sprung mass
$m_u$	Unsprung mass
$F_s$	Force applying on the sprung mass
$\theta_{1_j}$	A passive component connecting $m_u$ and the platform, where $j = 1, 2$
$\theta_{2_j}$	A passive component connecting $m_u$ and $m_s$ , where $j = 1, 2$
$\theta_{3_j}$	A passive component connecting $m_u$ and the piezo actuator, where $j = 1, 2$
$z_s$	Displacement of the sprung mass
$z_u$	Displacement of the unsprung mass
$z_r$	Displacement of the platform
$z_a$	Displacement output of the piezo actuator
$\gamma$	Transfer function from input voltage to the displacement ( $z_a - z_s$ )
CHECKED!!!	to be checked !!!!!!!!

Table 5.2: Signal Representation of The Full Table

Symbol	Signal Representation
Exogenous disturbance $w$	$[F_s, T_\theta, T_\phi, z_{r1}, z_{r2}, z_{r3}, z_{r4}]^T$
Regulated output $z$	$[z_s, z_\theta, z_\phi, z_{u1}, z_{u2}, z_{u3}, z_{u4}]^T$
Actuator input $u$	$[u_1, u_2, u_3, u_4]^T$
Measured output $y$	$[\ddot{z}_s, \ddot{z}_\theta, \ddot{z}_\phi, D_1, D_2, D_3, D_4]^T$

## 5.2 Controller Design

### 5.2.1 Design of $\tilde{U}_2$

The annihilated output  $\tilde{U}_2$  can be calculated from the inverse of  $\hat{P}_{21}$  in (1.2).

### 5.2.2 Design of $K_1$

The stabilizing controller  $K_1$  is constructed by MATLAB `ncfsyn` function, and  $K_1^{w_i}$  ( $i = 1, 2, 3, 4, 5, 6, 7$ ) are shown in Appendix from (A.7) to (A.13).

## 5.3 Simulation

After LFT form of the equations of motion is derived, the numerical model can be calculated by substituting all values in Table 5.3. Then we can generate some disturbances to simulate the vibrational situation. The disturbances  $w$  are given in equation from (5.18) to (5.24) and also shown in Figure 5.2.

$$\left\{ \begin{array}{ll} F_s = 10000\sin(\pi t) & (\text{unit} : N) \end{array} \right. \quad (5.18)$$

$$\left\{ \begin{array}{ll} T_\phi = 1000000\sin(2\pi t) & (\text{unit} : N * m) \end{array} \right. \quad (5.19)$$

$$\left\{ \begin{array}{ll} T_\phi = 3000000\sin(3\pi t) & (\text{unit} : N * m) \end{array} \right. \quad (5.20)$$

$$\left\{ \begin{array}{ll} z_{r_1} = 1.9\sin(2.12\pi t) & (\text{unit} : m) \end{array} \right. \quad (5.21)$$

$$\left\{ \begin{array}{ll} z_{r_2} = 2.1\sin(2.42\pi t) & (\text{unit} : m) \end{array} \right. \quad (5.22)$$

$$\left\{ \begin{array}{ll} z_{r_3} = 2.2\sin(2.42\pi t) & (\text{unit} : m) \end{array} \right. \quad (5.23)$$

$$\left\{ \begin{array}{ll} z_{r_4} = 2.3\sin(2.30\pi t) & (\text{unit} : m) \end{array} \right. \quad (5.24)$$

First, we observe the open-loop system of the full table, as shown in Figure 5.3.

The closed-loop system constructed by designing  $\tilde{U}_2^{w_i}$ , and  $K_1^{w_i}$ , where  $i = 1, 2, 3, 4, 5, 6, 7$ , has the following corresponding annihilated outputs  $\tilde{y}^{w_i}$ , as shown in Figure 5.4.

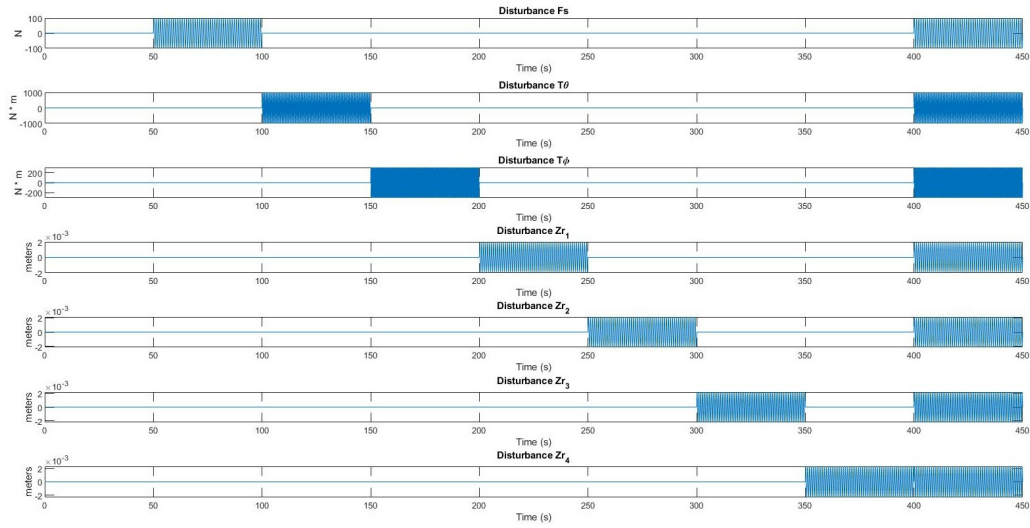


Figure 5.2: Exogenous Disturbances

Table 5.3: Parameters in The Full Table

Symbol	Value	Unit
$m_s$	19.0322	kg
$m_u$	11.5250	kg
$c_1$	373.558	Ns/m
$c_2$	289.247	Ns/m
$c_3$	446.353	Ns/m
$k_1$	$2.435\ 84 \times 10^5$	N/m
$k_2$	$2.022\ 63 \times 10^5$	N/m
$k_3$	$5.815\ 08 \times 10^5$	N/m
Others	other parameters in full table ?	???
$\gamma$	$\frac{0.0005662}{s+272.2}$	

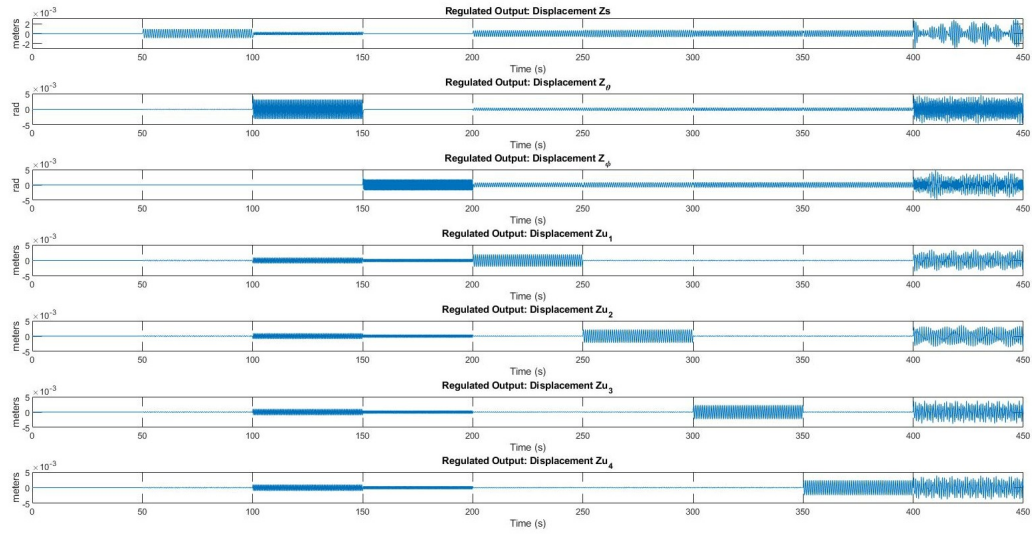


Figure 5.3: Outputs of An Open-loop System

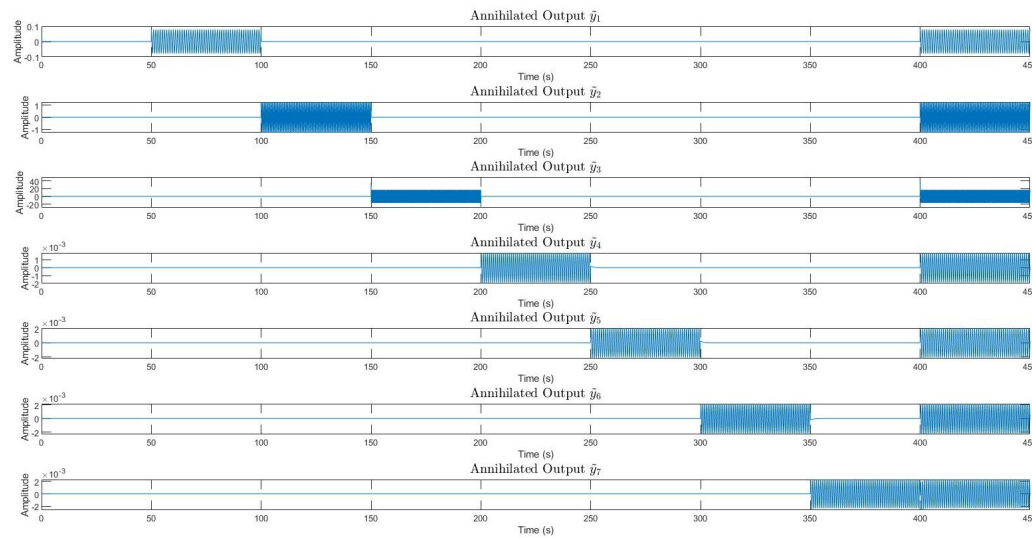


Figure 5.4: Annihilated Outputs

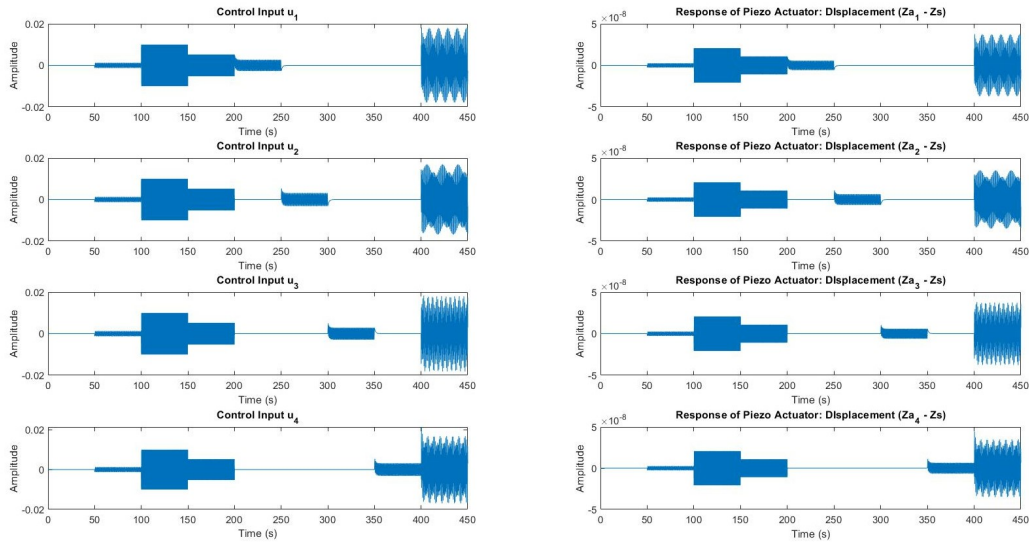


Figure 5.5: Response of Piezo Actuators

Also, because the purpose of the piezo actuator is to reduce the exogenous signal  $w$ , its output response matters in my simulation, as shown in Figure 5.5.

In my simulation, if only the steady state is considered, it can be observed that the maximum amplitude of  $(z_a - z_s)$  are approximately  $3 \times 10^{-8}$  meter for all four piezo actuators.

### 5.3.1 Vibration Reduction

The importance of my research is to reduce the regulated outputs  $z$ , so, here, I compare the open-loop and closed-loop system in Figure 5.6.

For the duration from 425 to 450 seconds, the vibration reduction is significant when seven controllers are open.

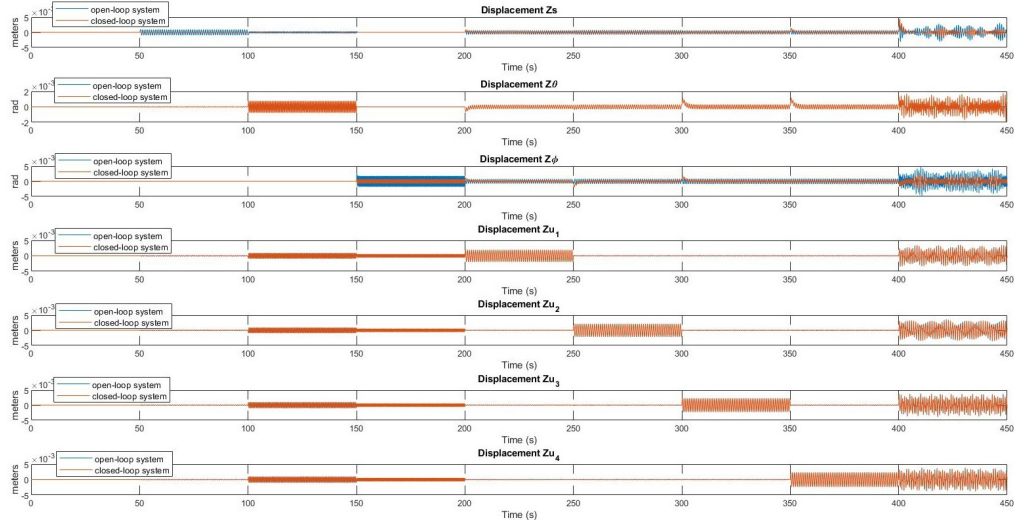


Figure 5.6: Regulated Outputs of Open- and Closed-loop System.

Table 5.4: Vibration Reduction of The Regulated Outputs

	$z_s$	$z_\theta$	$z_\phi$	$z_{u_1}$	$z_{u_2}$	$z_{u_3}$	$z_{u_4}$
only $K_1^{w_1}$ open	21.4%	0.04%	0.0%	0.38%	0.52%	-0.04%	-0.02%
only $K_1^{w_2}$ open	1.59%	61.3%	0.0%	0.05%	0.03%	1.32%	1.22%
only $K_1^{w_3}$ open	0.0%	0.0%	25.8%	-0.76%	-0.60%	-0.59%	-0.59%
only $K_1^{w_4}$ open	7.42%	0.61%	3.69%	2.48%	0.07%	0.21%	-0.27%
only $K_1^{w_5}$ open	10.6%	0.74%	2.94%	0.14%	2.58%	-0.06%	0.15%
only $K_1^{w_6}$ open	5.19%	0.95%	3.13%	0.04%	0.16%	2.19%	0.45%
only $K_1^{w_7}$ open	0.27%	1.09%	6.01%	0.42%	-0.23%	-0.41%	2.23%
all $K_1^{w_i}$ open	54.4%	70.3%	50.3%	2.69%	2.55%	2.64%	3.14%

# Chapter 6

## Disturbance Response Decoupling

### 6.1 General Control Configuration

Previously, a decoupling method proposed by Wang [16] incorporated the robust control method to the linear fractional transformation (LFT), and the closed-loop transfer function from one specific disturbance to the regulated outputs was fixed. That is, the controller was designed to improve the regulated outputs from the system excited by other disturbances. However, the number of disturbance sets should be expanded into higher-dimensional form if the system can be excited by more disturbances. Because of the limitations of multivariable control of LFT, it becomes necessary to modify the original algorithm. Therefore, input disturbance response decoupling (IDRD) is proposed to improve the regulated outputs  $z$  from the system excited by one disturbance  $\omega_1$ . In other words, our IDRD for multivariable control of LFT provides a decoupling scheme for the improvement from one excitation of the system, and other disturbances have no effects on the control signals.

Consider an open-loop plant  $G = P_{11}$ , which is the transfer function from the disturbances  $\omega$  to the regulated outputs  $z$ , as shown in Figure 6.1. Also, consider a generalized plant  $P$  in terms of linear fractional transformation (LFT) of a controller  $K$  as shown in Figure 6.2. Because of the analysis of closed-loop

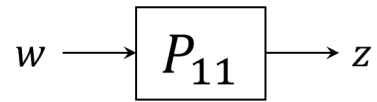


Figure 6.1: Open-loop System

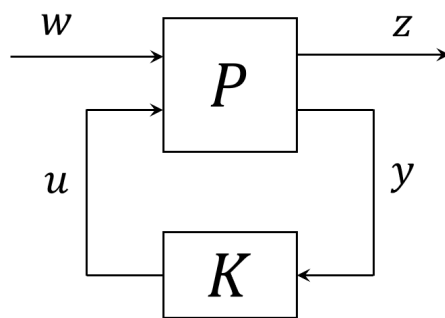


Figure 6.2: General Control Configuration

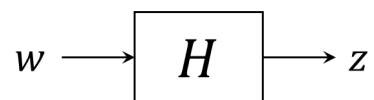


Figure 6.3: Closed-loop System

performance given the controller, we merge  $K$  into the interconnection structure and obtain the system  $H = F_l(P, K)$  as shown in Figure 6.3.

## 6.2 Review of Controller Parameterization

Controller parameterization is a fundamental problem in control theory. If the set of stabilizing controllers for a given plant is parameterized, then the parameters of the controllers become a function of a single variable. In this section, we will review some techniques for controller parameterization.

$$\begin{pmatrix} z \\ y \end{pmatrix} = \begin{pmatrix} P_{11} & P_{12} \\ P_{21} & P_{22} \end{pmatrix} \begin{pmatrix} w \\ u \end{pmatrix} \quad (6.1)$$

Suppose the generalized plant  $P$  is stabilizable. Since  $P_{11}$ ,  $P_{12}$ ,  $P_{21}$ , and  $P_{22}$  defined in (6.1) share the same unstable poles [18] [19], it can be proved that the stabilizing controller  $K$  is an internally-stabilizing controller for  $P$  if and only if  $K$  is an internally-stabilizing controller for  $P_{22}$ . Let  $P_{22} = NM^{-1} = \tilde{M}^{-1}\tilde{N}$  be the right and left coprime stable rational matrix of  $P_{22}$  and

$$\begin{pmatrix} \tilde{X} & -\tilde{Y} \\ -\tilde{N} & \tilde{M} \end{pmatrix} \begin{pmatrix} M & Y \\ N & X \end{pmatrix} = \begin{pmatrix} I & 0 \\ 0 & I \end{pmatrix} \quad (6.2)$$

be the corresponding Bezout identities, where all matrices in (6.2) belong to  $\mathbb{RH}_\infty$ , and the set of all stabilizing controllers which stabilizes  $P_{22}$  and  $P$  are given by

$$K = F_l(K_0, Q), Q \in \mathbb{RH}_\infty \quad (6.3)$$

where

$$K_0 = \begin{pmatrix} \tilde{X}^{-1}\tilde{Y} & -\tilde{X}^{-1} \\ X^{-1} & X^{-1}N \end{pmatrix}. \quad (6.4)$$

Since the closed-loop transfer function  $H$  is

$$H = F_l(P, K) = P_{11} + P_{12}K(I - P_{22}K)^{-1}P_{21}, \quad (6.5)$$

we have

$$H = T_1 - T_2QT_3 \quad (6.6)$$

where

$$K(I - P_{22}K)^{-1} = (Y - MQ)\tilde{M}, \quad (6.7)$$

$$T_1 = P_{11} + P_{12}Y\tilde{M}P_{21} \quad (6.8)$$

$$T_2 = P_{12}M \quad (6.9)$$

$$T_3 = \tilde{M}P_{21} \quad (6.10)$$

which is an affine parameterization of all internally-stable closed-loop systems.

### 6.3 Input Disturbance Response Decoupling (IDRD)

**Definition 1.** Assume that an open-loop system  $G = P_{11}$  is stable in (6.1) shown in Figure 6.1. Also, consider a generalized plant  $P$  excited by the  $n$  disturbances, namely  $\omega = [\omega_1, \omega_2, \dots, \omega_n]^T$ . If the controller  $K$  shown in Figure 6.2 improves the closed-loop  $H_{\omega_1 \rightarrow z}$  without changing other  $H_{\omega_j \rightarrow z}$ , where  $j = 2, 3, \dots, n$ , that is, if the response can be decoupled from one input disturbance, then we call this control method Input Disturbance Response Decoupling (IDRD).

Now, the objective of this section is to derive IDRD to improve the outputs from the system excited by one specific disturbances. In the following sections, we are going to see how IDRD improves  $H_{\omega_1 \rightarrow z}$  and how IDRD keeps other  $H_{\omega_j \rightarrow z}$  the same.

#### 6.3.1 Q-Parameterization (Youla)

A parameterization of all stabilizing controllers for the plant  $P(s)$  is given by [20], [16]

$$K = (Y - MQ)(X - NQ)^{-1} \quad (6.11)$$

$$= (\tilde{X} - Q\tilde{N})^{-1}(\tilde{Y} - Q\tilde{M}) \quad (6.12)$$

where  $Q$  is any stable transfer function and all matrices in (6.11) and (6.12) satisfy the Bezout identities (6.2) for the left and right coprime factorization.

The  $Q$ -parameterization is useful for controller synthesis [20]. First of all, the search over all  $K$ 's is replaced by a search over stable  $Q$ 's. Besides, all closed-loop transfer functions is in the form of (6.6), so they are affine in  $Q$ . This further simplifies the optimization problem.

**Example 6.3.1.** In (6.6), we can see  $Q$  parameterization. Once  $Q$  is determined, a corresponding controller  $K$  can be found by setting  $M = \tilde{M} = I$ ,  $N = \tilde{N} = P_{22}$ ,  $X = \tilde{X} = I$ , and  $Y = \tilde{Y} = 0$ . Then we have

$$K = -(I - QP_{22})^{-1}Q \quad (6.13)$$

**Theorem 6.3.1.** Consider a stabilizable generalized plant  $P$  in the configuration of (6.1) and Figure 6.2. All stabilizing controllers  $K$  is designed in the form of (6.11) and (6.12) with  $Q$  in (6.14) such that  $H_{\omega_j \rightarrow z_1} = G_{\omega_j \rightarrow z_1}$ .

$$\begin{pmatrix} V_1 \\ V_2 \\ V_3 \\ \vdots \\ V_m \end{pmatrix} Q = \begin{pmatrix} Q_{11} \\ -Q_{22}\tilde{U}_2 + \sum_{j=1}^n Q_{2j}\tilde{U}_j \\ -Q_{33}\tilde{U}_3 + \sum_{j=1}^n Q_{3j}\tilde{U}_j \\ \vdots \\ -Q_{mn}\tilde{U}_n + \sum_{j=1}^n Q_{mj}\tilde{U}_j \end{pmatrix} \quad (6.14)$$

Where  $j = 2, 3, \dots, n$ ,  $n$  is the number of exogenous disturbances, and  $m$  is the number of regulated outputs. Also,  $U$  and  $V$  are unimodular matrices, where

$$U = \begin{pmatrix} U_1, U_2, \dots, U_n \end{pmatrix} \quad (6.15)$$

$$V^T = \begin{pmatrix} V_1, V_2, \dots, V_m \end{pmatrix} \quad (6.16)$$

, and

$$\tilde{U}^T = U^{-T} = \begin{pmatrix} \tilde{U}_1, \tilde{U}_2, \dots, \tilde{U}_n \end{pmatrix} \quad (6.17)$$

$$\tilde{V} = V^{-1} = \begin{pmatrix} \tilde{V}_1, \tilde{V}_2, \dots, \tilde{V}_m \end{pmatrix}. \quad (6.18)$$

*Proof.* Wang [16] has proved that for any polynomial matrix  $T \in \mathbb{RH}_\infty$ , there exists a left normalrank factorization (lnf) and a right normalrank factorization (rnf) of  $T$ . Therefore,  $T_2$  and  $T_3$  in (6.6) can be factorized as follows:

$$T_{2j} = EV_j \quad (6.19)$$

$$T_{3j} = U_jF \quad (6.20)$$

Suppose  $M = T_2QT_3$ . Now we are going to prove  $M_{\omega_j \rightarrow z_1} = 0$  if and only if the parameterization of  $Q$  in (6.14) is satisfied.

First, suppose that  $M_{\omega_j \rightarrow z_1} = 0$ . By substituting (6.19) and (6.20) into  $M_{\omega_j \rightarrow z_1}$ , we have

$$E_jV_jQU_jF_j = 0 \quad (6.21)$$

where  $j = 2, 3, \dots, n$ . Because  $E$  has full column normalrank, and because  $F$  has full row normalrank, (6.21) is equivalent to (6.22).

$$V_jQU_j = 0 \quad (6.22)$$

Thus, we have the following form:

$$V_2Q \begin{pmatrix} U_1, U_2, \dots, U_n \end{pmatrix} = \begin{pmatrix} Q_{21}, 0, Q_{23}, \dots, Q_{2n} \end{pmatrix} \quad (6.23)$$

$$V_3Q \begin{pmatrix} U_1, U_2, \dots, U_n \end{pmatrix} = \begin{pmatrix} Q_{31}, Q_{32}, 0, \dots, Q_{3n} \end{pmatrix} \quad (6.24)$$

$$V_mQ \begin{pmatrix} U_1, U_2, \dots, U_n \end{pmatrix} = \begin{pmatrix} Q_{m1}, Q_{m2}, Q_{m3}, \dots, 0 \end{pmatrix} \quad (6.25)$$

Suppose  $V_1Q = Q_{11}$ . Then we have proven the  $Q$  parameterization expressed in (6.14).

Now, we want to prove this in the opposite direction. Suppose we have known the expression of  $Q$  in (6.14). Then intuitively (6.22) holds. Then we can multiply some lnf and rnf to get the result, same as in (6.21). Therefore, we have proven  $M_{\omega_j \rightarrow z_1} = 0$  as a result for  $j = 2, 3, \dots, n$ . ■

**Theorem 6.3.2.** Consider a stabilizable generalized plant  $P$  in the configuration of (6.1) and Figure 6.2. All stabilizing controllers  $K$  is designed in the form of (6.11) and (6.12) with  $Q$  in (6.26) such that  $H_{\omega_j \rightarrow z_1} = G_{\omega_j \rightarrow z_1}$ .

$$\begin{pmatrix} V_1 \\ \hat{V}_2 \end{pmatrix} Q = \begin{pmatrix} Q_{11} \\ \hat{Q}_2 \tilde{U} \end{pmatrix} \quad (6.26)$$

Where  $\hat{V}_2 = [V_2, V_3, \dots, V_m]^T$ ,  $\tilde{U} = [\tilde{U}_1, \tilde{U}_2, \dots, \tilde{U}_n]^T$ , and

$$\hat{Q}_2 = \begin{pmatrix} Q_{21} & 0 & Q_{23} & \cdots & Q_{2m} \\ Q_{31} & Q_{32} & 0 & \cdots & Q_{3m} \\ \vdots & & & & \vdots \\ Q_{m1} & Q_{m2} & Q_{m3} & \cdots & 0 \end{pmatrix} \quad (6.27)$$

*Proof.* Here, we factorize the submatrix of (6.14) to generalize Theorem 6.3.1.

$$\hat{Q}_2 \tilde{U} = \begin{pmatrix} -Q_{22} \tilde{U}_2 + \sum_{j=1}^n Q_{2j} \tilde{U}_j \\ -Q_{33} \tilde{U}_2 + \sum_{j=1}^m Q_{3j} \tilde{U}_j \\ \vdots \\ -Q_{mn} \tilde{U}_n + \sum_{j=1}^n Q_{mj} \tilde{U}_j \end{pmatrix} \quad (6.28)$$

Because there are more entries in  $\hat{Q}_2$  than ones in  $\tilde{U}$ , it is possible to find  $\hat{Q}_2$  such that  $U = \tilde{U}^{-1}$  is also unimodular. Then, in a similar way, we can prove that all stabilizing controllers  $K$  can be designed in the form of (6.11) and (6.12) with  $Q$  in (6.26) if and only if  $H_{\omega_j \rightarrow z_1} = G_{\omega_j \rightarrow z_1}$ . ■

### 6.3.2 Decoupling Effect

**Theorem 6.3.3.** Let the open-loop system  $G = P_{11}$  is stable. Assume  $K_0$  in (6.4) is zero. There exists  $\tilde{U}_1 \in \mathbb{RH}_\infty$  such that all stabilizing controllers requiring  $H_{\omega_j \rightarrow z} = G_{\omega_j \rightarrow z}$ , where  $j = 2, 3, \dots, n$ , can be parameterized as

$$K = -(I - \hat{Q}_2 \tilde{U}_1 P_{22})^{-1} \hat{Q}_2 \tilde{U}_1 \quad (6.29)$$

for  $\hat{Q}_2 \in \mathbb{RH}_\infty$ , where  $U_j$ , is defined in (6.20), and  $\tilde{U}$  is defined in (6.17).

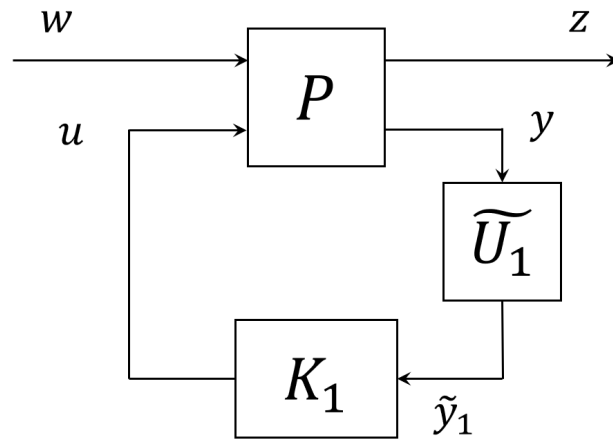


Figure 6.4: Control Structure of IDR D

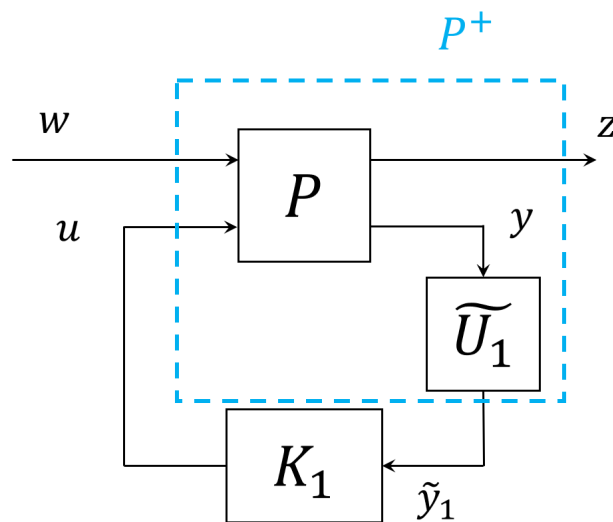


Figure 6.5: Control Structure of IDR D

*Proof.* By substituting  $Q = \hat{Q}_2 \tilde{U}_1$  into (6.13), then we get the result of (6.29). ■

**Theorem 6.3.4.** Let the open-loop system  $G = P_{11}$  is stable. Assume  $K_0$  in (6.4) is zero. Let  $U_j, j = 2, 3, \dots, n$  be defined in Theorem 6.3.3. Then we have  $K = K_1 \tilde{U}_1$ , where  $K_1$  is a stabilizing controller for  $\tilde{U}_1 P_{22}$ .

*Proof.* In Section 6.2, we conclude that  $K$  stabilizes  $P$  if and only if  $K$  stabilizes  $P_{22}$ . Apparently, it implies that  $K_1$  stabilizes  $P^+$  if and only if  $K_1$  stabilizes  $\tilde{U}_1 P_{22}$ , where  $P^+$  is defined in Figure 6.5. ■

**Theorem 6.3.5.** Let the open-loop system  $G = P_{11}$  is stable. Assume  $K_0$  in (6.4) is zero. Also consider the control configuration in Figure 6.6 with generalized plant  $P$  given by (6.1). If the design of  $\tilde{U}_1$  satisfies (6.30), where  $\tilde{U}_1$  is defined in (6.15) and (6.17), then the closed-loop  $H_{\omega_j \rightarrow z}$  remains the same as the open-loop  $G_{\omega_j \rightarrow z}$ , where  $j = 2, 3, \dots, n$ .

$$\tilde{U} = P_{21}^{-1} \quad (6.30)$$

*Proof.* From (6.5), the close-loop system  $H_{\omega \rightarrow z}$  in Figure 6.6 can be rearranged as:

$$H_{\omega \rightarrow z} = P_{11} + P_{12}(I - K_1 \tilde{U}_1 P_{22})^{-1} K_1 \tilde{U}_1 P_{21} \quad (6.31)$$

If  $\tilde{U} P_{21} = I$ , then

$$R = \tilde{U} P_{21} = \begin{pmatrix} \tilde{U}_1 \\ \tilde{U}_2 \\ \vdots \\ \tilde{U}_m \end{pmatrix} P_{21} = \begin{pmatrix} 1 & 0 & 0 & \cdots & 0 \\ 0 & 1 & 0 & \cdots & 0 \\ \vdots & & & & \vdots \\ 0 & 0 & 0 & \cdots & 1 \end{pmatrix} = \begin{pmatrix} r_1 \\ r_2 \\ \vdots \\ r_m \end{pmatrix} \quad (6.32)$$

where each row vector  $r_j$  has zero entries except for the  $j$ -th entry ( $r_{jj} = 1$ ). If we take  $\tilde{U}_1$ , then (6.31) can be simplified into

$$H_{\omega \rightarrow z} = P_{11} + P_{12}(I - K_1 \tilde{U}_1 P_{22})^{-1} K_1 r_1 \quad (6.33)$$

which means that  $H_{\omega_1 \rightarrow z}$  will be changed, and that the other  $H_{\omega_j \rightarrow z}$  will be fixed. ■

## 6.4 Output Disturbance Response Decoupling (ODRD)

**Definition 2.** Assume that an open-loop system  $G = P_{11}$  is stable in (6.1) shown in Figure 6.1. Also, consider a generalized plant  $P$  has  $m$  regulated outputs, namely  $z = [z_1, z_2, \dots, z_m]^T$ . If the controller  $K$  shown in Figure 6.2 improves the closed-loop  $H_{\omega \rightarrow z_1}$  without changing other  $H_{\omega \rightarrow z_j}$ , where  $j = 2, 3, \dots, m$ , that is, if each output of the system, which is excited by many disturbances, can be individually discussed, then we call this control method Output Disturbance Response Decoupling (ODRD).

Now, the objective of this section is to derive ODRD to improve single output from the system excited by various disturbances. In the following sections, we are going to see how ODRD improves  $H_{\omega \rightarrow z_1}$  and how ODRD keeps other  $H_{\omega \rightarrow z_j}$  the same.

### 6.4.1 Q-Parameterization (Youla)

**Lemma 6.4.1.** Consider a stabilizable generalized plant  $P$  in the configuration of (6.1) and Figure 6.2. All stabilizing controllers  $K$  is designed in the form of (6.11) and (6.12) with  $Q$  in (6.34) such that  $H_{\omega_1 \rightarrow z_j} = G_{\omega_1 \rightarrow z_j}$ .

$$Q \begin{pmatrix} U_1 \\ \hat{U}_2 \end{pmatrix} = \begin{pmatrix} Q_{11} \\ \tilde{V} \hat{Q}_2 \end{pmatrix} \quad (6.34)$$

Where  $\hat{U}_2 = [U_2, U_3, \dots, U_n]$ ,  $\tilde{V} = [\tilde{V}_1, \tilde{V}_2, \dots, \tilde{V}_m]$ , and

$$\hat{Q}_2 = \begin{pmatrix} Q_{21} & 0 & Q_{23} & \cdots & Q_{2n} \\ Q_{31} & Q_{32} & 0 & \cdots & Q_{3n} \\ \vdots & & & & \vdots \\ Q_{m1} & Q_{m2} & Q_{m3} & \cdots & 0 \end{pmatrix} \quad (6.35)$$

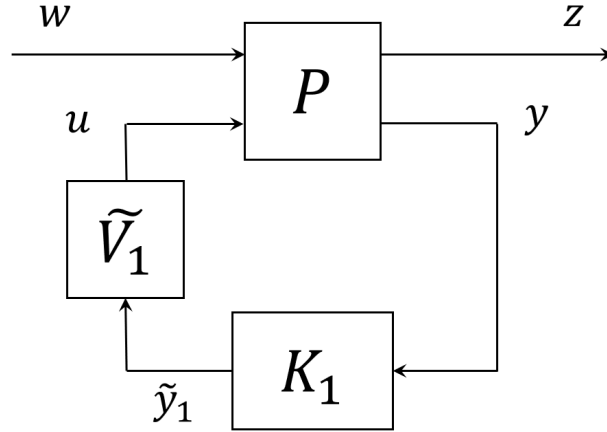


Figure 6.6: Control Structure of ODRD

$$\tilde{V} \hat{Q}_2 = \begin{pmatrix} -\tilde{V}_2 Q_{22} + \sum_{j=1}^m \tilde{V}_j Q_{j2} \\ -\tilde{V}_3 Q_{33} + \sum_{j=1}^m \tilde{V}_j Q_{j3} \\ \vdots \\ -\tilde{V}_m Q_{mm} + \sum_{j=1}^m \tilde{V}_j Q_{jn} \end{pmatrix} \quad (6.36)$$

*Proof.* Because there are more entries in  $\hat{Q}_2$  than ones in  $\tilde{V}$ , it is possible to find  $\hat{Q}_2$  such that  $V = \tilde{V}^{-1}$  is also unimodular. Then, in a similar way, we can prove that all stabilizing controllers  $K$  can be designed in the form of (6.11) and (6.12) with  $Q$  in (6.34) if and only if  $H_{\omega_1 \rightarrow z_j} = G_{\omega_1 \rightarrow z_j}$ . ■

### 6.4.2 Decoupling Effect

**Theorem 6.4.2.** Let the open-loop system  $G = P_{11}$  is stable. Assume  $K_0$  in (6.4) is zero. There exists  $\tilde{V}_1 \in \mathbb{RH}_\infty$  such that all stabilizing controllers requiring  $H_{\omega \rightarrow z_j} = G_{\omega \rightarrow z_j}$ , where  $j = 2, 3, \dots, m$ , can be parameterized as

$$K = -\tilde{V}_1 \hat{Q}_2 (I - P_{22} \tilde{V}_1 \hat{Q}_2)^{-1} \quad (6.37)$$

for  $\hat{Q}_2 \in \mathbb{RH}_\infty$ , where  $V_j$ , is defined in (6.19), and is defined in (6.18).

*Proof.* By substituting  $Q = \tilde{V}_1 \hat{Q}_2$  into (6.13), then we get the result of (6.37). ■

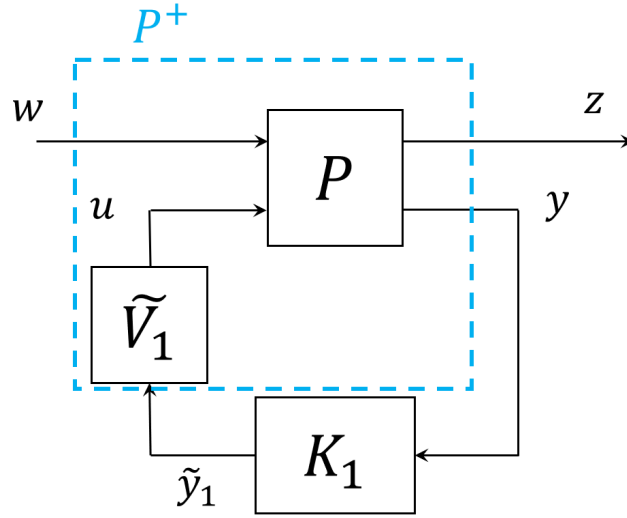


Figure 6.7: Control Structure of ODRD

**Theorem 6.4.3.** Let the open-loop system  $G = P_{11}$  be stable. Assume  $K_0$  in (6.4) is zero. Let  $V_j, j = 2, 3, \dots, m$  be defined in Theorem 6.4.2. Then we have  $K = \tilde{V}_1 K_1$ , where  $K_1$  is a stabilizing controller for  $P_{22} \tilde{V}_1$ .

*Proof.* In Section 6.2, we conclude that  $K$  stabilizes  $P$  if and only if  $K$  stabilizes  $P_{22}$ . Apparently, it implies that  $K_1$  stabilizes  $P^+$  if and only if  $K_1$  stabilizes  $P_{22} \tilde{V}_1$ , where  $P^+$  is defined in Figure 6.7. ■

**Theorem 6.4.4.** Let the open-loop system  $G = P_{11}$  be stable. Assume  $K_0$  in (6.4) is zero. Also consider the control configuration in Figure 6.6 with generalized plant  $P$  given by (6.1). If the design of  $\tilde{V}_1$  satisfies (6.38), where  $\tilde{V}_1$  is defined in (6.16) and (6.18), then the closed-loop  $H_{\omega \rightarrow z_j}$  remains the same as the open-loop  $G_{\omega \rightarrow z_j}$ , where  $j = 2, 3, \dots, m$ .

$$\tilde{V} = P_{12}^{-1} \quad (6.38)$$

*Proof.* From (6.5), the close-loop system  $H_{\omega \rightarrow z}$  in Figure 6.6 can be rearranged as:

$$H_{\omega \rightarrow z} = P_{11} + P_{12} \tilde{V}_1 K_1 (I - P_{22} \tilde{V}_1 K_1)^{-1} P_{21} \quad (6.39)$$

If  $P_{12}\tilde{V} = I$ , then

$$C = P_{12}\tilde{V} = P_{12} \begin{pmatrix} \tilde{V}_1 & \tilde{V}_2 & \cdots & \tilde{V}_m \end{pmatrix} = \begin{pmatrix} 1 & 0 & 0 & \cdots & 0 \\ 0 & 1 & 0 & \cdots & 0 \\ \vdots & & & & \vdots \\ 0 & 0 & 0 & \cdots & 1 \end{pmatrix} = \begin{pmatrix} c_1 & c_2 & \cdots & c_m \end{pmatrix} \quad (6.40)$$

where each column vector  $c_j$  has zero entries except for the  $j$ -th entry ( $c_{jj} = 1$ ). If we take  $\tilde{V}_1$ , then (6.39) can be simplified into

$$H_{\omega \rightarrow z} = P_{11} + c_1 K_1 (I - P_{22} \tilde{V}_1 K_1)^{-1} P_{21} \quad (6.41)$$

which means that  $H_{\omega \rightarrow z_1}$  will be changed, and that the other  $H_{\omega \rightarrow z_j}$  will be fixed. ■



# Chapter 7

## Output DRD Applied to A Half Table

### 7.1 Output Disturbance Response Decoupling (ODRD)

Previously, we have derived disturbance response decoupling [16]. Now, we rename it as input disturbance response decoupling (IDRD) because the purpose of IDRD is to fix the transfer function  $T_{\omega_1 \rightarrow z}$ , and we pay attention to one specific disturbance in this control structure. However, there is another issue to be considered: if there are many external disturbances from the environment, can we fix at least one response? That is, no matter what the environmental disturbances are, the system still has the same response  $z_1$ . Therefore, it becomes necessary to derive another decoupling form to improve the system response, and in this chapter, a new objective is to fix the transfer function from all disturbances to one regulated output  $z_1$ . In the following pages, output disturbance response decoupling (ODRD) will be introduced to fix the transfer function  $T_{\omega \rightarrow z_1}$ .

$$\begin{pmatrix} z \\ y \end{pmatrix} = \begin{pmatrix} P_{11} & P_{12} \\ P_{21} & P_{22} \end{pmatrix} \begin{pmatrix} w \\ u \end{pmatrix} \quad (7.1)$$

$$(open-loop)G = P_{11} = \begin{pmatrix} G_1 & G_2 \\ G_3 & G_4 \end{pmatrix}; \quad (closed-loop)H = \begin{pmatrix} H_1 & H_2 \\ H_3 & H_4 \end{pmatrix} \quad (7.2)$$

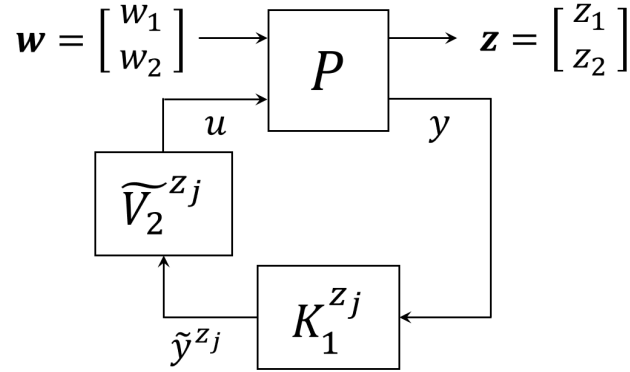


Figure 7.1: Control Structure of ODRD

**Definition 3.** Let  $G$  be open-loop stable in (7.2) and in (7.1). Consider a right annihilator of  $P_{12,1}$ , namely  $\tilde{V}_2$ , where  $P_{12,1}$  is  $[P_{12,11}, P_{12,12}, \dots, P_{12,1n}]^T$  and  $n$  is the number of actuators. The design of  $\tilde{V}_2$  is to fix  $T_{\omega \rightarrow z_1}$  in a closed-loop system. If (7.3) is satisfied, then we say we can fix the transfer function  $T_{\omega \rightarrow z_1}$ , and this is the spirit of output disturbance response decoupling (ODRD).

$$P_{12,1}\tilde{V}_2 = 0 \quad (7.3)$$

*Proof.* The general form of ODRD should be proved here, but I haven't finished it yet. ■

**Lemma 7.1.1.** Consider a special case of (7.1) with a specific dimension, as shown in Figure 7.1. Assume  $P_{11} \in \mathbb{R}^{2 \times 2}$ ,  $P_{12} \in \mathbb{R}^{2 \times 2}$ ,  $P_{21} \in \mathbb{R}^{1 \times 2}$ , and  $P_{22} \in \mathbb{R}^{1 \times 2}$ . Also, consider  $\tilde{V}_2 \in \mathbb{R}^{2 \times 1}$ . To satisfy the condition in (7.3),  $\tilde{V}_2$  can be designed as  $[-p_{12,12}, p_{12,11}]^T W$ , where  $W$  is a weighting function and  $W \in \mathbb{R}$ . Then,  $K_1 \in \mathbb{R}^1$  can be designed to stabilize  $P_{22}\tilde{V}_2$ .

*Proof.* The closed-loop system in Figure 7.1 can be simplified into a transfer function  $H$  from  $[\omega_1, \omega_2]^T$  to  $[z_1, z_2]^T$  described in (7.2), and we can derive  $H$  from MATLAB symbolic expression, where  $H_1, H_2, H_3$ , and  $H_4$  are described in (7.4):

$$H_1 = G_1 - \frac{1}{\Delta} K_1 P_{21,1} [P_{12,11}, P_{12,12}] [\tilde{V}_2^1, \tilde{V}_2^{21}]^T \quad (7.4)$$

$$H_2 = G_2 - \frac{1}{\Delta} K_1 P_{21,2} [P_{12,11}, P_{12,12}] [\tilde{V}_2^1, \tilde{V}_2^{21}]^T \quad (7.5)$$

$$H_3 = G_3 - \frac{1}{\Delta} K_1 P_{21,1} [P_{12,21}, P_{12,22}] [\tilde{V}_2^1, \tilde{V}_2^{21}]^T \quad (7.6)$$

$$H_4 = G_4 - \frac{1}{\Delta} K_1 P_{21,2} [P_{12,21}, P_{12,22}] [\tilde{V}_2^1, \tilde{V}_2^{21}]^T \quad (7.7)$$

Where

$$\Delta = K_1 [P_{22,1}, P_{22,2}] [\tilde{V}_2^1, \tilde{V}_2^{21}]^T - 1 \quad (7.8)$$

To fix  $T_{\omega \rightarrow z_1}$ , we have assumptions of  $G_1 = H_1$  and  $G_2 = H_2$ . Obviously, ODRD provides solutions for  $\tilde{V}_2$ . In the next section, we will apply ODRD to a half table by using this lemma with the same matrix dimension. ■

## 7.2 Dynamic Equations

A half-table model is used to study the dynamics of an optical table [1, 17]. Figure 7.2 illustrates the free body diagram, and its corresponding equations of motion can be derived as:

$$m_s \ddot{z}_s = F_s - u_{p_1} - u_{p_2} \quad (7.9)$$

$$I_\phi \ddot{z}_\phi = T_\phi - u_{p_1} l_1 + u_{p_2} l_2 \quad (7.10)$$

$$m_{u_1} \ddot{z}_{u_1} = u_{p_1} - \theta_{1_1} (z_{u_1} - z_{r_1}) \quad (7.11)$$

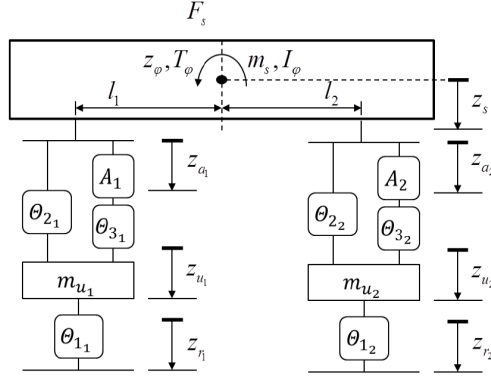


Figure 7.2: Half Table [12]

$$m_{u_2} \ddot{z}_{u_2} = u_{p_2} - \theta_{1_2} (z_{u_2} - z_{r_2}) \quad (7.12)$$

where  $u_{p_1}$  and  $u_{p_2}$  are defined as:

$$u_{p_1} = \theta_{2_1} (z_s + l_1 z_\phi - z_{u_1}) + \theta_{3_1} (z_{a_1} - z_{u_1}) \quad (7.13)$$

$$u_{p_2} = \theta_{2_2} (z_s - l_2 z_\phi - z_{u_2}) + \theta_{3_2} (z_{a_2} - z_{u_2}) \quad (7.14)$$

where each parameter is defined in Table 7.1. And the displacement output of  $z_a$  can be substituted by the transfer function  $\gamma$ :

$$z_{a_1} - z_s - l_1 z_\phi = \gamma u_1 \quad (7.15)$$

$$z_{a_2} - z_s + l_2 z_\phi = \gamma u_2 \quad (7.16)$$

Then, the above equations can be formulated into LFT form. The next thing to do is to simplify the half table problem. Because of the limitations of ODRD described in Lemma 7.1.1, we suppose that the force  $F_s$  and torque  $T_\phi$  does not exist. In the following simulation, we will only discuss a simplified case with two disturbances from an uneven road, and all signals are defined in Table 7.2.

Table 7.1: Symbol Meanings of The Half Table

Symbol	Meaning
$m_s$	Sprung mass
$m_u$	Unsprung mass
$F_s$	Force applying on the sprung mass
$\theta_{1_j}$	A passive component connecting $m_u$ and the platform, where $j = 1, 2$
$\theta_{2_j}$	A passive component connecting $m_u$ and $m_s$ , where $j = 1, 2$
$\theta_{3_j}$	A passive component connecting $m_u$ and the piezo actuator, where $j = 1, 2$
$z_s$	Displacement of the sprung mass
$z_{u_j}$	Displacement of the unsprung mass, where $j = 1, 2$
$z_{r_j}$	Displacement of the platform, where $j = 1, 2$
$z_{a_j}$	Displacement output of the piezo actuator, where $j = 1, 2$
$\gamma_j$	Transfer function from input voltage to the displacement ( $z_{a_j} - z_s$ )

Table 7.2: Signal Representation of A Simplified Half Table

Symbol	Signal Representation
Exogenous disturbance $w$	$[z_{r_1}, z_{r_2}]^T$
Regulated output $z$	$[z_s, z_\phi]^T$
Actuator input $u$	$[u_1, u_2]^T$
Measured output $y$	$z_{u_1}$

Table 7.3: Parameters in The Half Table

Symbol	Value	Unit
$m_s$	10.8090	kg
$m_{u_1}$	9.451	kg
$m_{u_2}$	12.630	kg
$c_{1_j}$	373.558	Ns/m
$c_{2_j}$	289.247	Ns/m
$c_{3_j}$	446.353	Ns/m
$k_{1_j}$	$2.435\ 84 \times 10^5$	N/m
$k_{2_j}$	$2.022\ 63 \times 10^5$	N/m
$k_{3_j}$	$5.815\ 08 \times 10^5$	N/m
$l_1$	0.225	m
$l_2$	0.225	m
$\gamma$	$\frac{0.0005662}{s+272.2}$	

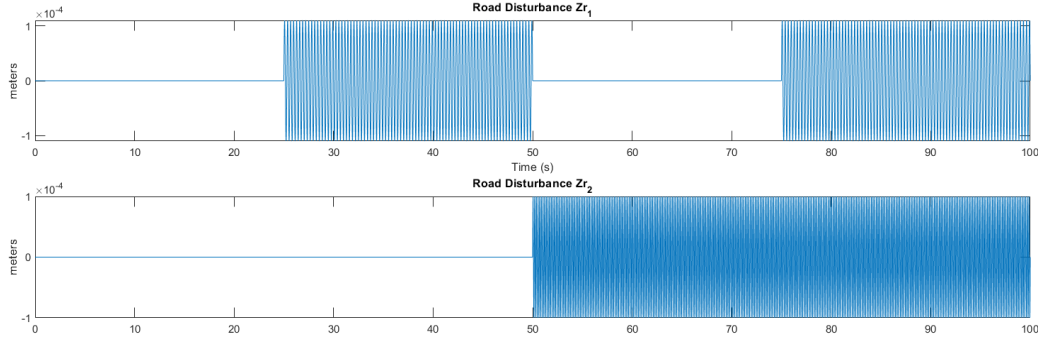


Figure 7.3: Exogenous Disturbances

## 7.3 Simulation

Note: The output of PZT in this section is unconstrained, i.e., the voltage  $u$  can be maximized without considering the limitation of the PZT.

After LFT form of the equations of motion is derived, the numerical model can be calculated by substituting all values in Table 7.3. Then we can generate some disturbances to simulate the vibrational situation. The disturbances  $w$  are given in equation (7.17) and (7.18) and also shown in Figure 7.3.

$$\begin{cases} z_{r_1} = 0.00011 \sin(6.6\pi t) & (\text{unit : m}) & (7.17) \\ z_{r_2} = 0.00010 \sin(12.0\pi t) & (\text{unit : m}) & (7.18) \end{cases}$$

### 7.3.1 Controller Design

To fix  $T_{\omega \rightarrow z_1}$ , we can design a transfer function  $\tilde{V}_2^{z_1}$  by using Lemma 7.1.1. Also, to fix  $T_{\omega \rightarrow z_2}$ , we can design another  $\tilde{V}_2^{z_2}$ . The stabilizing controller  $K_1$  can be designed by using MATLAB command `ncfsyn`, and  $K_1$  is designed to stabilize  $P_{22}\tilde{V}_2$ .

In the following three sub-sections, we will discuss three different ODRD by fixing  $T_{\omega \rightarrow z_1}$ ,  $T_{\omega \rightarrow z_2}$ , and fixing both  $T_{\omega \rightarrow z_1}$  and  $T_{\omega \rightarrow z_2}$ .

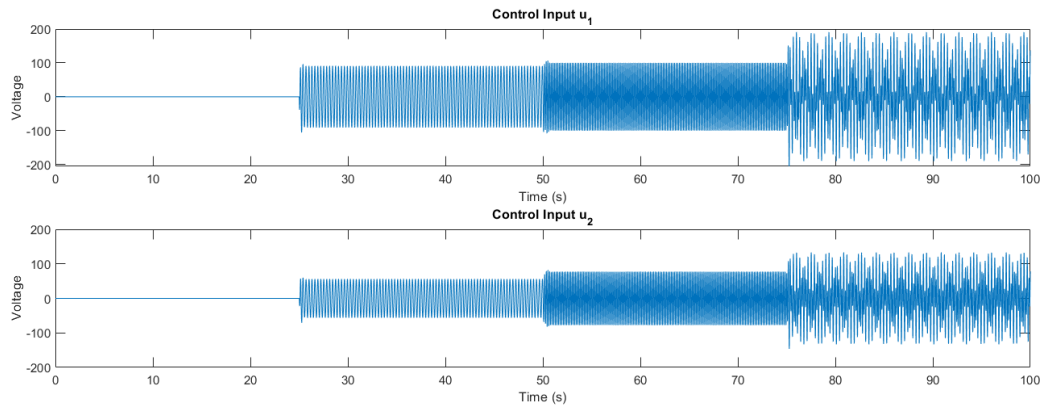


Figure 7.4: Response of Piezo Actuators (1st ODRD).

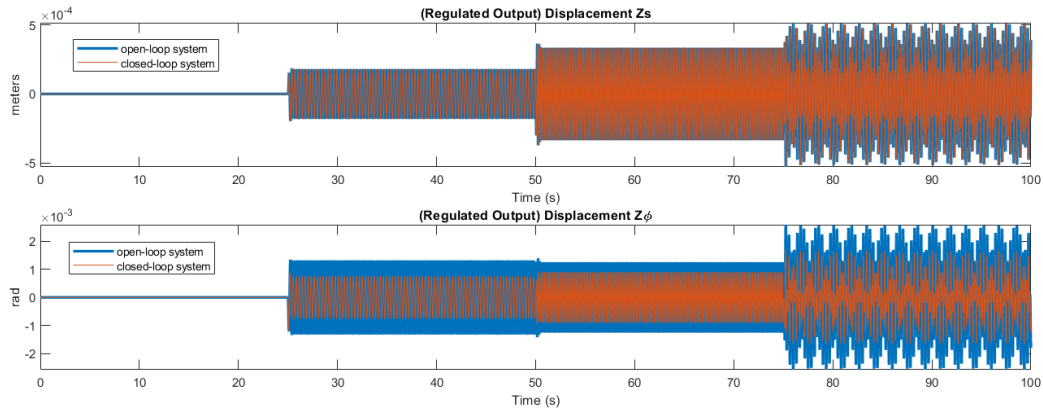


Figure 7.5: Regulated Outputs of Open- and Closed-loop System (1st ODRD).

### 7.3.2 First ODRD

First, we can observe the system response by fixing  $T_{\omega \rightarrow z_1}$ . We can see control signals for each actuator PZT in Figure 7.4 and system response in Figure 7.5. Besides, in ODRD structure, we fix the transfer function  $T_{\omega \rightarrow z_1}$ . In other words,  $T_{\omega \rightarrow z_2}$  might be changed, and it is possible that the vibrational pattern of the regulated output  $z_2$  can be improved. Here, we observe the system response only from 80 to 100 seconds, and the 2-norm of each regulated signal is calculated in Table 7.4 and Table 7.5.

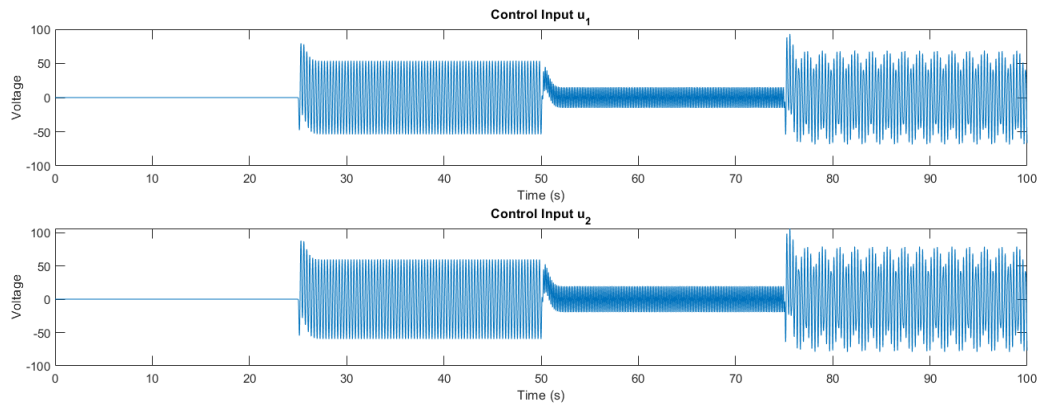


Figure 7.6: Response of Piezo Actuators (2nd ODRD).

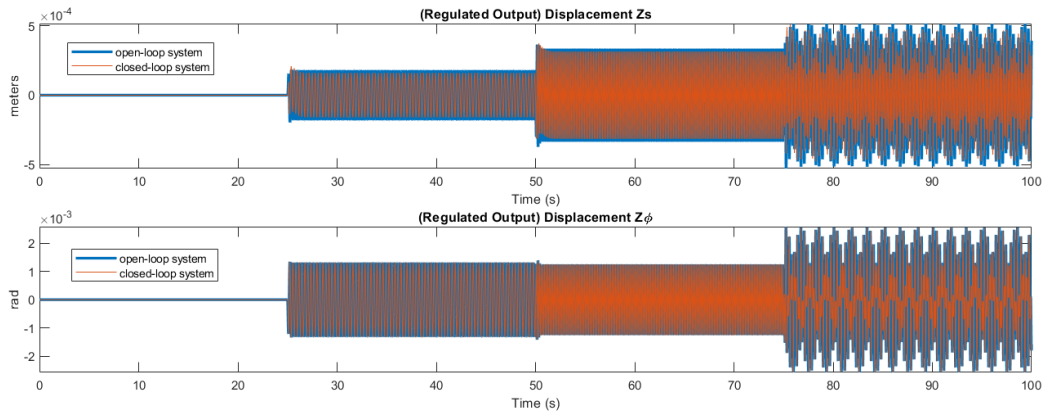


Figure 7.7: Regulated Outputs of Open- and Closed-loop System (2nd ODRD).

### 7.3.3 Second ODRD

Next, we are interested in fixing another transfer function, namely  $T_{\omega \rightarrow z_2}$ . We can see control signals for each actuator PZT in Figure 7.6 and system response in Figure 7.7. Besides, the 2-norm of each regulated signal from 80 to 100 seconds is calculated in Table 7.4 and Table 7.5.

### 7.3.4 Hybrid ODRD

Next, we are interested in fixing both transfer functions, i.e., both  $T_{\omega \rightarrow z_1}$  and  $T_{\omega \rightarrow z_2}$ . We can see control signals for each actuator PZT in Figure 7.8 and system response

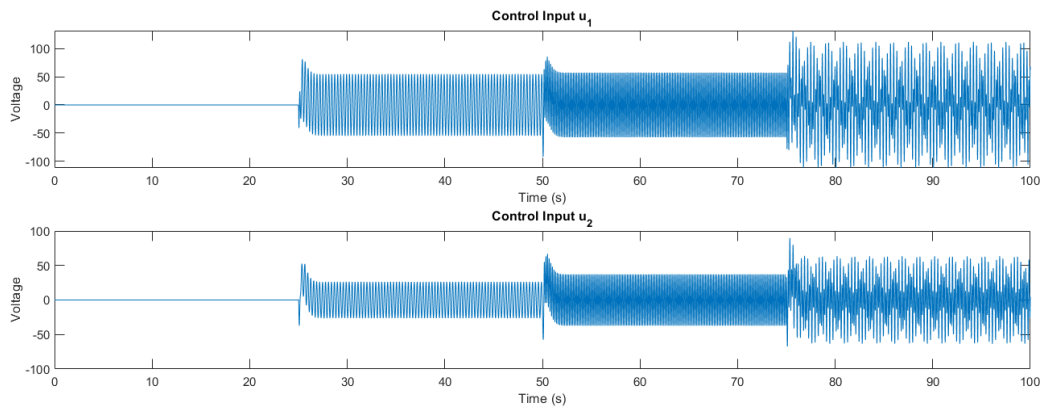


Figure 7.8: Response of Piezo Actuators (Hybrid ODRD).

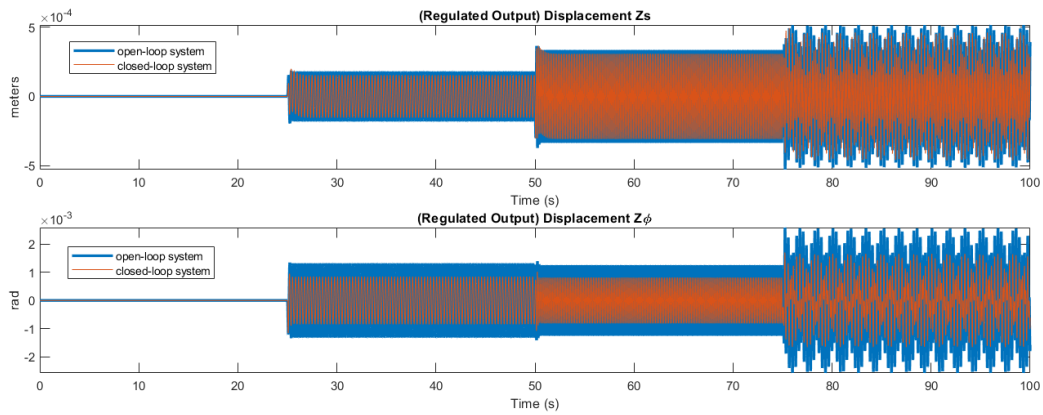


Figure 7.9: Regulated Outputs of Open- and Closed-loop System (Hybrid ODRD).

in Figure 7.9. Besides, the 2-norm of each regulated signal from 80 to 100 seconds is calculated in Table 7.4 and Table 7.5.

Table 7.4: Vibration Reduction of The Regulated Output  $z_s$ .

$z_s$	30 - 50 sec	55 - 75 sec	80 - 100 sec
only $\tilde{V}_2^{z_1}$ open	0%	0%	0%
only $\tilde{V}_2^{z_2}$ open	11.1%	6.2%	7.2%
Both $\tilde{V}_2^{z_j}$ open ( $j = 1, 2$ )	15.1%	8.1%	9.6%

Table 7.5: Vibration Reduction of The Regulated Output  $z_\phi$ .

$z_\phi$	30 - 50 sec	55 - 75 sec	80 - 100 sec
only $\tilde{V}_2^{z_1}$ open	42.3%	27.9%	35.1%
only $\tilde{V}_2^{z_2}$ open	0%	0%	0%
Both $\tilde{V}_2^{z_j}$ open ( $j = 1, 2$ )	35.9%	35.1%	35.5%

# Chapter 8

## Input-Output DRD Applied to A Half Table

### 8.1 Input-Output Disturbance Response Decoupling (IODRD)

Previously, we have derived IDR and ODR, which are two algorithms designed to fix  $T_{\omega_1 \rightarrow z}$  and  $T_{\omega \rightarrow z_1}$ , respectively. How about fixing  $T_{\omega_1 \rightarrow z_1}$ ? It will be interesting to observe the modification of a transfer function from one specific input to another regulated output. In this chapter, a new algorithm is proposed: Input-Output Disturbance Response Decoupling (abbreviated as IODRD), and the objective is to fix  $T_{\omega_1 \rightarrow z_1}$ .

**Definition 4.** Let  $G$  be open-loop stable in (7.2) and in (7.1). Consider a left annihilator of  $P_{21,1}$ , namely  $\tilde{U}_2$ , where  $P_{21,1}$  is  $[P_{21,11}, P_{21,21}, \dots, P_{21,m1}]^T$  and  $m$  is the number of measured outputs. The design of  $\tilde{U}_2$  is to fix  $T_{\omega_1 \rightarrow z}$  in a closed-loop system. Besides, consider a right annihilator of  $P_{12,1}$ , namely  $\tilde{V}_2$ , where  $P_{12,1}$  is  $[P_{12,11}, P_{12,12}, \dots, P_{12,1n}]^T$  and  $n$  is the number of actuators. The design of  $\tilde{V}_2$  is to fix  $T_{\omega \rightarrow z_1}$  in a closed-loop system. If both (8.1) and (8.2) are satisfied, then we say we can fix the transfer function  $T_{\omega_1 \rightarrow z_1}$ , and this is the spirit of input-output

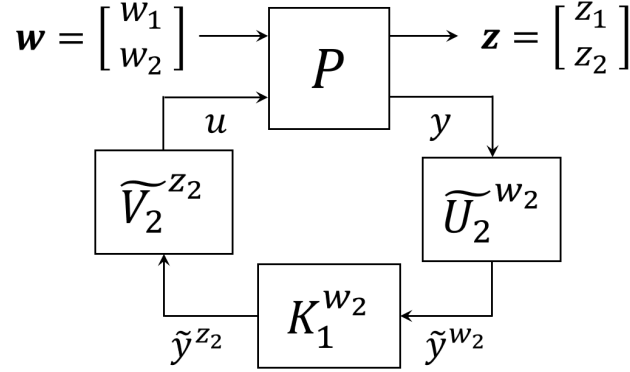


Figure 8.1: Control Structure of IODRD

disturbance response decoupling (IODRD).

$$P_{12,1}\tilde{V}_2 = 0 \quad (8.1)$$

$$\tilde{U}_2 P_{21,1} = 0 \quad (8.2)$$

*Proof.* The general form of IODRD should be proved here, but I haven't finished it yet. ■

**Lemma 8.1.1.** Consider a special case of (7.1) with a specific dimension, as shown in Figure 8.1. Assume  $P_{11} \in \mathbb{R}^{2 \times 2}$ ,  $P_{12} \in \mathbb{R}^{2 \times 2}$ ,  $P_{21} \in \mathbb{R}^{2 \times 2}$ , and  $P_{22} \in \mathbb{R}^{2 \times 2}$ . Also, consider  $\tilde{V}_2 \in \mathbb{R}^{2 \times 1}$  and  $\tilde{U}_2 \in \mathbb{R}^{1 \times 2}$ . To satisfy two conditions, namely (8.1) and (8.2),  $\tilde{U}_2$  can be designed as  $[-p_{21,21}, p_{21,11}]$ , and  $\tilde{V}_2$  can be designed as  $[-p_{12,12}, p_{12,11}]^T$ . Then,  $K_1 \in \mathbb{R}^1$  can be designed to stabilize  $\tilde{U}_2 P_{22} \tilde{V}_2$ .

*Proof.* The closed-loop system in Figure 8.1 can be simplified into a transfer function  $H$  from  $[\omega_1, \omega_2]^T$  to  $[z_1, z_2]^T$  described in (7.2), and we can derive  $H$  from MATLAB symbolic expression, where  $H_1, H_2, H_3$ , and  $H_4$  are described in (8.3):

$$H_1 = G_1 - \frac{1}{\Delta} [\tilde{U}_2^1, \tilde{U}_2^2] [P_{21,11}, P_{21,21}]^T K_1 [P_{12,11}, P_{12,12}] [\tilde{V}_2^1, \tilde{V}_2^2]^T \quad (8.3)$$

$$H_2 = G_2 - \frac{1}{\Delta} [\tilde{U}_2^1, \tilde{U}_2^2] [P_{21,12}, P_{21,22}]^T K_1 [P_{12,11}, P_{12,12}] [\tilde{V}_2^1, \tilde{V}_2^2]^T \quad (8.4)$$

$$H_3 = G_3 - \frac{1}{\Delta} [\tilde{U}_2^1, \tilde{U}_2^2] [P_{21,11}, P_{21,21}]^T K_1 [P_{12,21}, P_{12,22}] [\tilde{V}_2^1, \tilde{V}_2^2]^T \quad (8.5)$$

$$H_4 = G_4 - \frac{1}{\Delta} [\tilde{U}_2^1, \tilde{U}_2^2] [P_{21,12}, P_{21,22}]^T K_1 [P_{12,21}, P_{12,22}] [\tilde{V}_2^1, \tilde{V}_2^2]^T \quad (8.6)$$

Where

$$\Delta = K_1 [1, 1] [P_{22} \circ R] [1, 1]^T - 1 \quad (8.7)$$

Where  $R = \tilde{V}_2 \tilde{U}_2$  and the symbol  $\circ$  is the hadamard product performing element-wise multiplication. ■

In the next section, we will apply IODRD to a half table by using this Lemma 8.1.1 with the same matrix dimension.

## 8.2 Dynamic Equations

The equations of motion derived in Chapter 7 can be formulated into LFT form. The next thing to do is to simplify the half table problem. Because of the limitations of IODRD described in Lemma 8.1.1, we suppose that the force  $F_s$  and torque  $T_\phi$  have no effect on the half table. In the following simulation, we will only discuss a simplified case with two disturbances excited from an uneven road, and all signals are defined in Table 8.1.

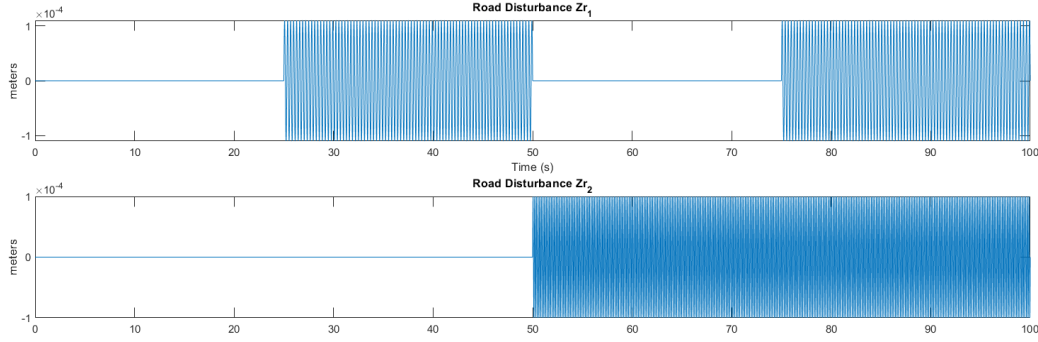


Figure 8.2: Exogenous Disturbances

### 8.3 Simulation

Note: The output of PZT in this section is unconstrained, i.e., the voltage  $u$  can be maximized without considering the limitation of the PZT.

After LFT form of the equations of motion is derived, we can generate some disturbances to simulate the vibrational situation. The disturbances  $w$  are given in equation (8.8) and (8.9) and also shown in Figure 8.2.

$$\begin{cases} z_{r_1} = 0.00011 \sin(6.6\pi t) & (\text{unit : m}) & (8.8) \\ z_{r_2} = 0.00010 \sin(12.0\pi t) & (\text{unit : m}) & (8.9) \end{cases}$$

#### 8.3.1 Controller Design

To fix  $T_{\omega \rightarrow z_1}$ , we can design a transfer function  $\tilde{V}_2^{z_1}$  by using Lemma 8.1.1. Also, to fix  $T_{\omega \rightarrow z_2}$ , we can design another  $\tilde{V}_2^{z_2}$ . In addition, to fix  $T_{\omega_1 \rightarrow z}$ , we can design a transfer function  $\tilde{U}_2^{\omega_1}$ . Also, to fix  $T_{\omega_2 \rightarrow z}$ , we can design another  $\tilde{U}_2^{\omega_2}$ . The stabilizing controller  $K_1$  can be designed by using MATLAB command `ncfsyn`, and  $K_1$  is designed to stabilize  $\tilde{U}_2 P_{22} \tilde{V}_2$ .

In the following results, we will see how IODRD improves the regulated outputs  $z$  by changing four transfer function  $T_{\omega_i \rightarrow z_j}$ , where  $i, j \in [1, 2]$

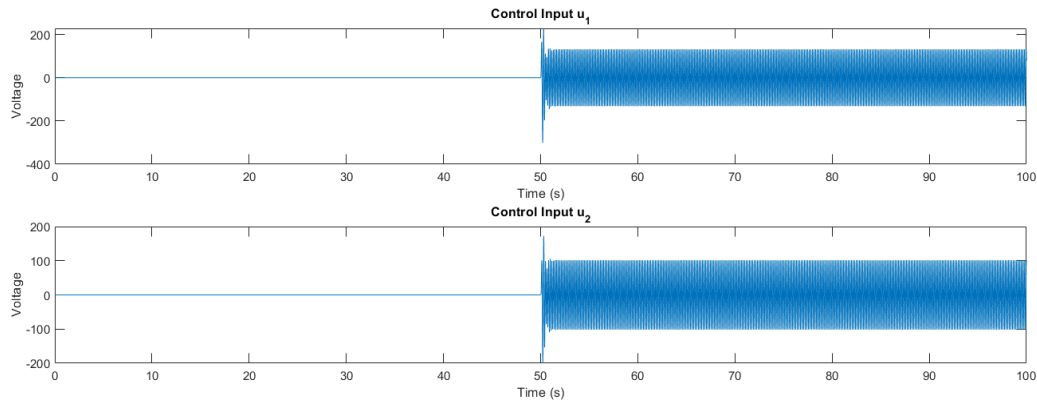


Figure 8.3: Response of Piezo Actuators (1st IODRD).

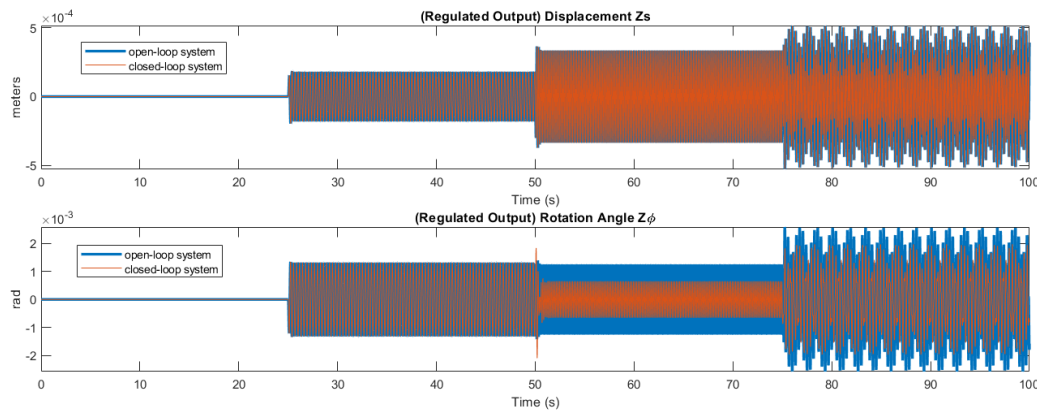


Figure 8.4: Regulated Outputs of Open- and Closed-loop System (1st IODRD).

### 8.3.2 First IODRD

First, we can observe the system response by modifying  $T_{\omega_2 \rightarrow z_2}$ . We can see control signals for each actuator PZT in Figure 8.3 and system response in Figure 8.4. Besides, in the IODRD structure, other transfer functions are fixed, and only the regulated output  $z_2$  is improved because IODRD modifies the transfer function  $T_{\omega_2 \rightarrow z_2}$ .

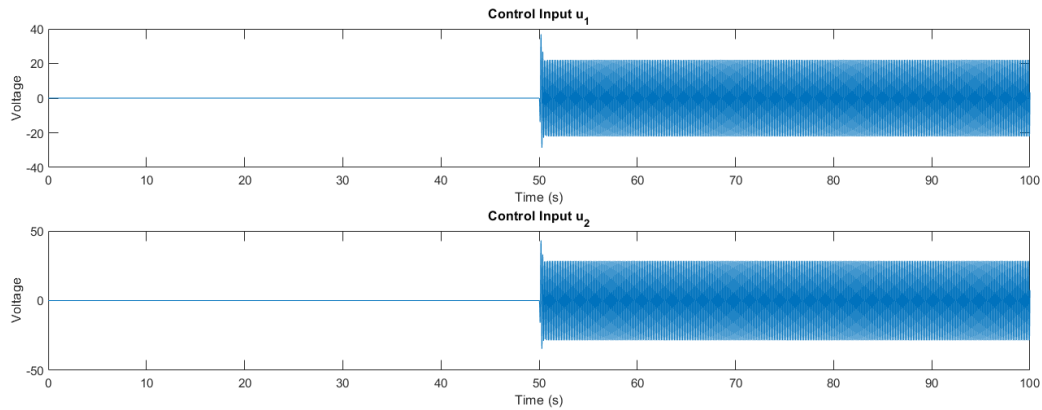


Figure 8.5: Response of Piezo Actuators (2nd IODRD).

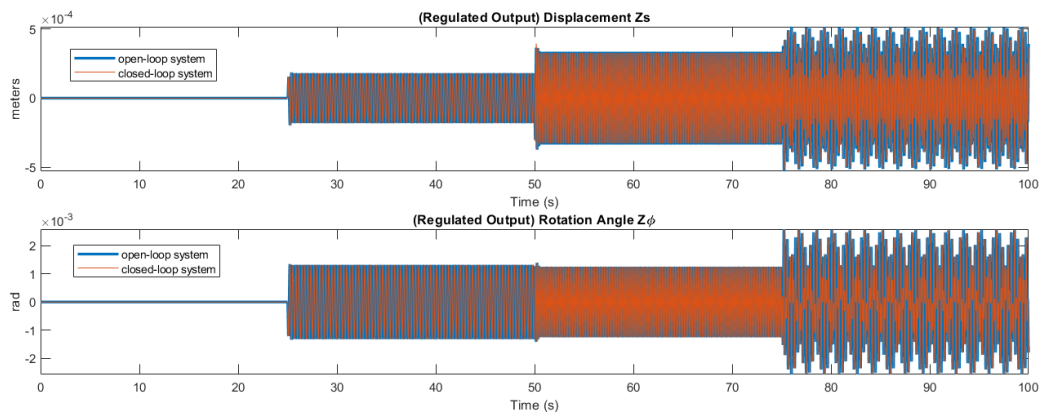


Figure 8.6: Regulated Outputs of Open- and Closed-loop System (2nd IODRD).

### 8.3.3 Second IODRD

Second, we can observe the system response by modifying  $T_{\omega_2 \rightarrow z_1}$ . We can see control signals for each actuator PZT in Figure 8.5 and system response in Figure 8.6. Besides, in the IODRD structure, other transfer functions are fixed, and only the regulated output  $z_1$  is improved because IODRD modifies the transfer function  $T_{\omega_2 \rightarrow z_1}$ .

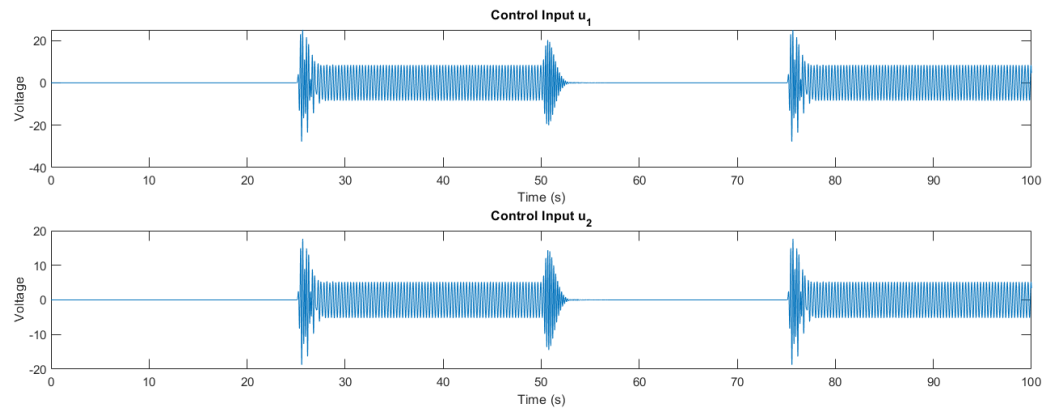


Figure 8.7: Response of Piezo Actuators (3rd IODRD).

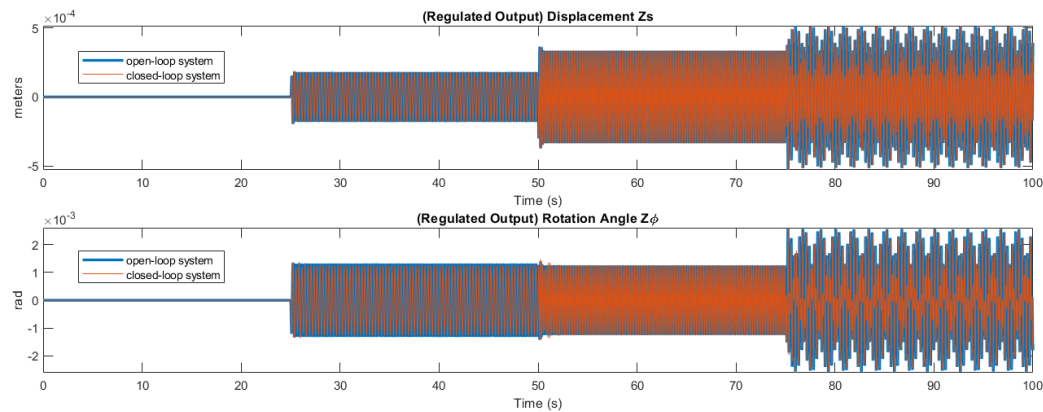


Figure 8.8: Regulated Outputs of Open- and Closed-loop System (3rd IODRD).

### 8.3.4 Third IODRD

Third, we can observe the system response by modifying  $T_{\omega_1 \rightarrow z_2}$ . We can see control signals for each actuator PZT in Figure 8.7 and system response in Figure 8.8. Besides, in the IODRD structure, other transfer functions are fixed, and only the regulated output  $z_2$  is improved because IODRD modifies the transfer function  $T_{\omega_1 \rightarrow z_2}$ .

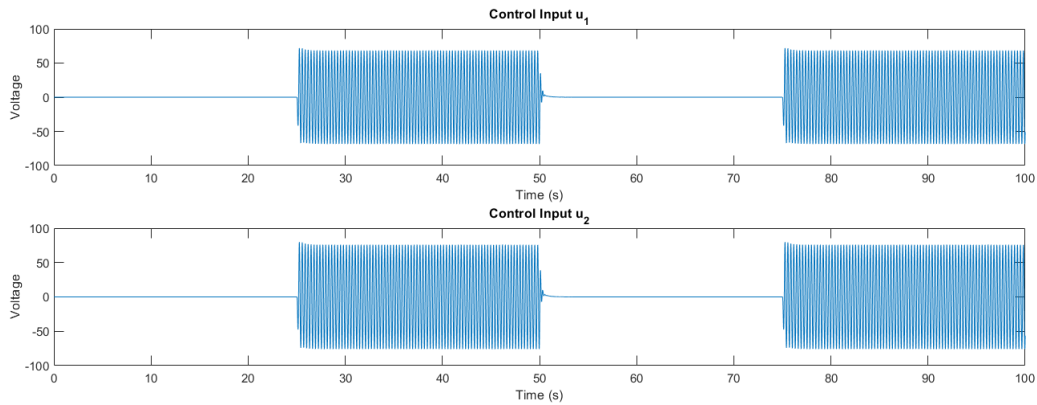


Figure 8.9: Response of Piezo Actuators (4th IODRD).

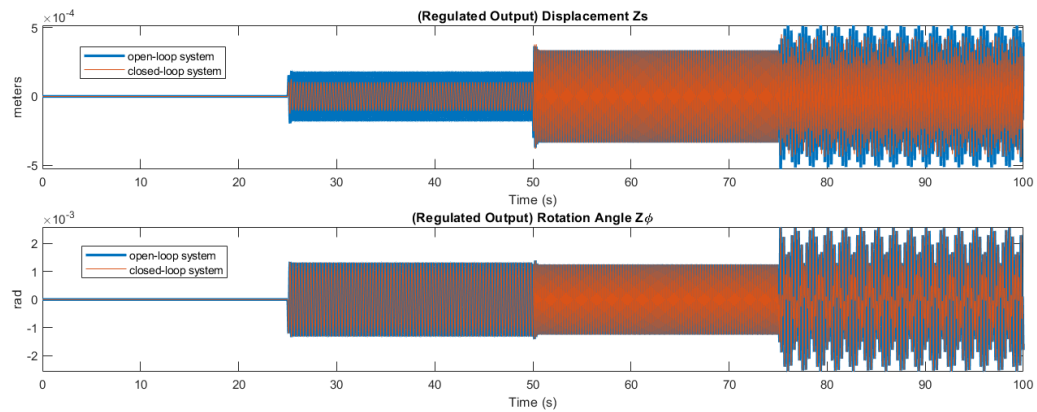


Figure 8.10: Regulated Outputs of Open- and Closed-loop System (4th IODRD).

### 8.3.5 Fourth IODRD

Last but not least, we can observe the system response by modifying  $T_{\omega_1 \rightarrow z_1}$ . We can see control signals for each actuator PZT in Figure 8.9 and system response in Figure 8.10. Besides, in the IODRD structure, other transfer functions are fixed, and only the regulated output  $z_1$  is improved because IODRD modifies the transfer function  $T_{\omega_1 \rightarrow z_1}$ .

Table 8.1: Signal Representation of A Simplified Half Table

Symbol	Signal Representation
Exogenous disturbance $w$	$[z_{r_1}, z_{r_2}]^T$
Regulated output $z$	$[z_s, z_\phi]^T$
Actuator input $u$	$[u_1, u_2]^T$
Measured output $y$	$[z_{u_1}, z_{u_2}]^T$

Table 8.2: Vibration Reduction of The Regulated Output  $z_s$ .

$z_s$	30 - 50 sec	55 - 75 sec	80 - 100 sec
1st IODRD	0%	0%	0%
2nd IODRD	0%	2.39%	1.84%
3rd IODRD	0%	0%	0%
4th IODRD	42.4%	0%	7.83%

Table 8.3: Vibration Reduction of The Regulated Output  $z_\phi$ .

$z_\phi$	30 - 50 sec	55 - 75 sec	80 - 100 sec
1st IODRD	0%	48.0%	19.1%
2nd IODRD	0%	0%	0%
3rd IODRD	4.04%	0%	2.10%
4th IODRD	0%	0%	0%



# Chapter 9

## Conclusions

### 9.1 Conclusions

This research has explored the effectiveness of disturbance response decoupling (DRD) strategies in the design and control of optical tables, emphasizing the critical need for vibration control in precision applications. By introducing and validating the Input DRD (IDRD) approach, we have demonstrated that it significantly decouples exogenous disturbances and reduces vibrations, enhancing the overall performance of optical tables. Our findings indicate that while the original DRD strategy effectively addresses specific disturbances, it requires modifications to generalize the relationship between multiple disturbances and outputs.

Through the development of Output DRD (ODRD) and Input-Output DRD (IODRD) strategies, we have laid the groundwork for a more comprehensive approach to vibration control in optical tables. Simulation results underscore the potential of these strategies to provide substantial improvements in stability and performance. Overall, this work contributes valuable insights to the field of vibration control, opening new avenues for optimizing the design and functionality of optical systems.

## 9.2 Future Work

Future research will focus on the experimental validation of the ODRD and IODRD strategies. This will involve designing a series of experiments to systematically evaluate their performance in real-world conditions, assessing their effectiveness in various operational environments. Additionally, we aim to explore the integration of advanced sensor technologies and adaptive control algorithms to further enhance disturbance decoupling capabilities.

Another avenue for future work includes the expansion of the current models to accommodate a wider range of disturbances, including environmental factors that may impact optical table performance. Investigating the scalability of these strategies to larger optical systems and different configurations will also be a key focus, as will the potential application of machine learning techniques to predict and mitigate disturbances dynamically.

Ultimately, this ongoing research seeks to refine vibration control methodologies, contributing to the advancement of optical technologies and their applications in various scientific and industrial fields.

# Appendix A

## Design of Stabilizing Controller $K_1$

This section shows all numerical values of my stabilizing controllers for quarter, half, and full table.

### A.1 Design of $K_1$ - Quarter Table

$$K_1^{w_1} = \frac{10s^4 + 10000}{s^5 + 10s^4 + 1000000} \quad (\text{A.1})$$

$$K_1^{w_2} = \frac{10s^4 + 10000}{s^5 + 10s^4 + 1000000} \quad (\text{A.2})$$

### A.2 Design of $K_1$ - Half Table

$$K_1^{w_1} = \frac{10s^4 + 10000}{s^5 + 10s^4 + 1000000} \quad (\text{A.3})$$

$$K_1^{w_2} = \frac{10s^4 + 10000}{s^5 + 10s^4 + 1000000} \quad (\text{A.4})$$

$$K_1^{w_3} = \frac{10s^4 + 10000}{s^5 + 10s^4 + 1000000} \quad (\text{A.5})$$

$$K_1^{w_4} = \frac{10s^4 + 10000}{s^5 + 10s^4 + 1000000} \quad (\text{A.6})$$

### A.3 Design of $K_1$ - Full Table

$$K_1^{w_1} = \frac{10s^4 + 10000}{s^5 + 10s^4 + 1000000} \quad (\text{A.7})$$

$$K_1^{w_2} = \frac{10s^4 + 10000}{s^5 + 10s^4 + 1000000} \quad (\text{A.8})$$

$$K_1^{w_3} = \frac{10s^4 + 10000}{s^5 + 10s^4 + 1000000} \quad (\text{A.9})$$

$$K_1^{w_4} = \frac{10s^4 + 10000}{s^5 + 10s^4 + 1000000} \quad (\text{A.10})$$

$$K_1^{w_5} = \frac{10s^4 + 10000}{s^5 + 10s^4 + 1000000} \quad (\text{A.11})$$

$$K_1^{w_6} = \frac{10s^4 + 10000}{s^5 + 10s^4 + 1000000} \quad (\text{A.12})$$

$$K_1^{w_7} = \frac{10s^4 + 10000}{s^5 + 10s^4 + 1000000} \quad (\text{A.13})$$

# **Appendix B**

## **Device Specification**

Table B.1: Specification of The Vertical Vibration Machine

Specifications	Parameters	Units
Platform mass	14	kg
Loading limit	100	kg
Loading area	400×400	mm <sup>2</sup>
Working frequency	0.1-30	Hz
Maximum zcceleration	0.5g	
Total stroke	0.4	m
Diameter of threads	25	mm
Screw pitch	10	mm/rev
Screw inertia	$1.2 \times 10^{-4}$	kg×m <sup>2</sup>
Output torque of the motor	4.9 / 20 (peak)	N×m
Motor pulse	8192	pulse/rev
Rotor inertia	$2.7 \times 10^{-4}$	kg×m <sup>2</sup>

Table B.2: Specification of P-844.20, Physik Instrumente [3]

Specifications	Parameters	Units
Travel range from 0 to 100 V	30	μm
Push force capacity	3000	N
Pull force capacity	700	N
Resonant frequency $f_0$ (no load)	12	kHz
Electrical capacitance	12	μF
Mass without cable	108	g
Length L	65	mm

Table B.3: Specification of E-663, Physik Instrumente [4]

Specifications	Parameters	Units
Channels	3	
Input voltage	-2 to 12	V
Minimum output voltage	-20 to 120	V
Peak output power per channel	14	W
Voltage gain	$10 \pm 0.1$	
Input impedance	100	k Ω
Mass	4.6	kg

Table B.4: Specification of AVM35-HF-7, Akribis [13]

Specifications	Parameters	Units
Stroke	7.00	mm
Force sensitivity (at mid stroke)	16.00	N/A
Back EMF constant	16.00	V/m/s
Peak force	72	N
Inductance	3.95	mH
Continuous current	0.90	A
Peak current	4.50	A
Power at peak force	188.3	W

Table B.5: Specification of OPA544, Texas Instruments [14]

Specifications	Parameters	Units
Range of input voltage	$\pm 6$	V
Range of power supply	$\pm 10$ to $\pm 35$	V
Maximum output current	2	A
Gain bandwidth	1.4	MHz
Open-loop gain	103	dB
Slew rate	8	V/ms

Table B.6: Specification of Accelerometer 731A/P31, Wilcoxon Research Inc. [7].

Specifications	Parameters	Units
Sensing element design	PZT ceramic / flexture	
Acceleration sensitivity, selectable	10, 100, 1000	V/g
Velocity sensitivity, selectable	0.1, 1, 10	V/in/sec
Vibration range, max	0.5 g peak	
Transverse sensitivity, max	1% of axial	
Noise	0.003	$\mu\text{g}/\sqrt{\text{Hz}}$
Frequency response (-3 dB)	0.05 - 100	Hz
Vibration limit	10g peak	

Table B.7: Specification of PR 750-050, Macro Sensors [9].

Specifications	Parameters	Units
Input voltage (nominal)	3.0	Vrms
Linearity error	$< \pm 0.25\%$ of full scale output	
Repeatability error	$< \pm 0.01\%$ of full scale output	
Nominal range	$\pm 1.25$	mm
Impedance, primary	400	$\Omega$

Table B.8: Specification of LVC-2500, Macro Sensors [9].

Specifications	Parameters	Units
Manufacturer	Macro Sensors	
Type	LVC-2500	
Input sensitivity range	0.055 to 5.5	Vrms
Full scale outputs	0 to $\pm 10$ V DC, 5 mA	
Output Non-linearity	$< \pm 0.01\%$ of full scale output	
Frequency response (-3dB), selectable	250, 500	Hz

Table B.9: Specification of MLP-200, Transducer Techniques [11].

Specifications	Parameters	Units
Capacity	200	lb
Natural ringing frequency	5200	Hz
Deflection inches	0.003	inch

Table B.10: Specification of NI PCI-6259 [15].

Analog Input		Analog Output	
Analog input channels	16 SE / 8 DI	Analog output channels	2
Nominal input ranges	$\pm 0.1, \pm 1, \pm 5, \pm 10$ V	Nominal output ranges	$\pm 5, \pm 10$ V
Maximum input range	$\pm 11$ V	Maximum output range	$\pm 11$ V
ADC resolution	16 bits	DAC resolution	16 bits
Input impedance	$> 10$ G $\Omega$	Output impedance	0.2 $\Omega$
Input bias current	$\pm 100$ pA	Current Drive	$\pm 5$ mA
Bandwidth (-3dB)	0.7 MHz		

Table B.11: Specification of NI PCIe-6323 [15].

Analog Input		Analog Output	
Analog input channels	32 SE / 16 DI	Analog output channels	4
Nominal input ranges	$\pm 0.2, \pm 1, \pm 5, \pm 10$ V	Nominal output ranges	$\pm 10$ V
Maximum input range	$\pm 11$ V	Maximum output range	$\pm 11$ V
ADC resolution	16 bits	DAC resolution	16 bits
Input impedance	$> 10$ G $\Omega$	Output impedance	$0.2$ $\Omega$
Input bias current	$\pm 100$ pA	Current Drive	$\pm 5$ mA
Bandwidth (-3dB)	0.7 MHz		



# Bibliography

- [1] Y.-H. Chen, “Multiple hybrid disturbance response decoupling applied to an optical table for vibration suppression,” Master’s thesis, National Taiwan University, 2021. [vii, 4, 15, 23, 35, 59](#)
  
- [2] P. Technology, “Tooling: Back to basics on die springs part 1,” 2020, last accessed 03 February 2022. [Online]. Available: <https://www.ptonline.com/> [vii, 5](#)
  
- [3] P. Instrumente, “P-844 preloaded piezo actuators,” last accessed 03 February 2022. [Online]. Available: <https://www.physikinstrumente.com/> [vii, xii, 6, 82](#)
  
- [4] —, “E-663 3-channel piezo amplifier,” last accessed 03 February 2022. [Online]. Available: <https://www.physikinstrumente.com/> [vii, xii, 6, 82](#)
  
- [5] MachineDesign, “What is a voice coil actuator?” 2018, last accessed 03 February 2022. [Online]. Available: <https://www.machinedesign.com/> [vii, 7](#)
  
- [6] R.-J. Li, Y.-J. Lei, Z.-X. Chang, L.-S. Zhang, and K.-C. Fan, “Development of a high-sensitivity optical accelerometer for low-frequency vibration measurement,” *Sensors*, vol. 18, no. 9, p. 2910, 2018. [vii, 8](#)
  
- [7] W. S. Technologies®, “Seismic accelerometer and power amplifier system 731a/p31,” last accessed 03 February 2022. [Online]. Available: <https://wilcoxon.com/> [vii, xii, 8, 83](#)

- [8] A. A. Circuits, "Introduction to linear variable differential transformers (lvdt)," 2021, last accessed 03 February 2022. [Online]. Available: <https://www.allaboutcircuits.com/> vii, 9, 10
- [9] M. Sensors, "General purpose - lvdt position sensors," last accessed 03 February 2022. [Online]. Available: <https://www.hgsind.com/> vii, xii, 10, 84
- [10] L. C. Central, "How a load cell works," last accessed 03 February 2022. [Online]. Available: <https://www.800loadcel.com/> vii, 11, 12
- [11] T. Techniques, "Mlp series," last accessed 03 February 2022. [Online]. Available: <https://www.transducertechniques.com/> vii, xii, 12, 84
- [12] S.-Y. Wu, "The applications of inverse disturbance response decoupling and mechatronic inerter networks to an optical table," Master's thesis, National Taiwan University, 2013. vii, viii, 16, 24, 37, 60
- [13] Akribis, "Avm series: Voice coil actuators," last accessed 03 February 2022. [Online]. Available: <http://www.akribis-sys.co.kr/> xii, 83
- [14] T. Instruments, "High-voltage, high-current operational amplifier (opa544)," last accessed 03 February 2022. [Online]. Available: <https://www.ti.com/> xii, 83
- [15] N. Instruments, "Multifunction i/o device manual," last accessed 03 February 2022. [Online]. Available: <https://www.ni.com/documentation/en/multifunction-io-device/> xii, 84, 85
- [16] F.-C. Wang, "Design and synthesis of active and passive vehicle suspensions," Ph.D. dissertation, University of Cambridge, 2001. 2, 43, 46, 48, 57
- [17] R.-Q. Zheng, "Hybrid disturbance response decoupling: Application to a vibration suppression structure," Master's thesis, National Taiwan University, 2019. 15, 23, 35, 59

- [18] K. Glover, D. Limebeer, J. Doyle, E. Kasenally, and M. G. Safonov, “A characterization of all solutions to the four block general distance problem,” *SIAM Journal on Control and Optimization*, vol. 29, no. 2, pp. 283–324, 1991. [45](#)
- [19] M. Green and D. J. Limebeer, *Linear robust control*. Courier Corporation, 2012. [45](#)
- [20] S. Skogestad and I. Postlethwaite, *Multivariable feedback control: analysis and design*. Citeseer, 2007, vol. 2. [46](#), [47](#)